ENHANCED MECHANICAL PROPERTIES OF POLYMERIC MATERIALS BY ADDING GRAPHENE OXIDE

Yangyang Guo

BSc (Chem)

Submitted in fulfilment of the requirements for the degree of

Master of Philosophy (Science)

Centre for Materials Science

School of Chemistry and Physics

Faculty of Science

Queensland University of Technology

2022

Keywords

Atomic Force Microscopy

Contact Stiffness

Electrospinning

Graphene Oxide Platelet

Hardness

Mechanical Property

Nanoindentation

Nanoparticles

Platelet Size Differentiation

Spider Silk Modelling

Young’s Modulu

Abstract

Polymer nanocomposites fabricated by dispersing nanofillers, or reinforcements have been found to have improved functional properties that are unachievable with a single material. Molecular modelling obtained via the experimental observation of polymeric nanocomposites is widely used to understand the complexity of intermolecular interactions in natural fibres. The case of the spider silk is particularly interesting as it has truly exceptional properties, but a clear understanding of this material is still missing.

Inspired by a well-known molecular model of spider dragline silk, I simulated its structure experimentally by using graphene oxide (GO) as nanofiller in polyvinylpyrrolidone (PVP) polymer matrix, to understand how GO platelets impact on the mechanical properties of the polymeric material in form of bulk material and nanofibers by varying (1) the platelet size and (2) the concentration of GO.

The differentiation of GO platelet size has been successfully achieved by ultrasonication and centrifugation techniques with investigations in different parameters. Atomic Force Microscopy (AFM) provides a measurement of the size and thickness of GO platelets, while Fourier Transform Infrared Spectroscopy (FT-IR) analyses the functional groups attached to the graphitic plane in GO. The concentration of treated GO supernatants has also been obtained by UV-Vis spectra and added to polymer by a simple solution mixing technique.

The composite material has been prepared into bulk material on a glass substrate and nanofibers via electrospinning process. The parameters of

electrospinning process have been extensively studied to achieve the desired fibre diameter.

Finally, the mechanical properties of the bulk material have been assessed including Young's modulus and Hardness using a nano-indenter. Given the challenges, three point bending tests have been attempted on nanofibers which however need further investigations in future research. Instead, conventional indentation tests have been performed on nanofibers which shows the effect of GO addition in polymer. Experimental and analytical results have shown that both the bulk polymer mixture and the nanofibers exhibit improved mechanical properties after the addition of GO platelets: the concentration of GO appears to have more prominent effect than the size.

This work is the first attempt to study the structure-property relationship at the nanoscale between PVP polymer and GO platelets in bulk and nanofiber form. The results will provide critical information to produce new super-elastic materials, with applications in medicine, for the development of artificial tendons and ligaments.

Table of Contents

List of Figures

List of Tables

List of Abbreviations

0D	Zero-dimension
1D	One-dimension
2D	Two-dimension
AFM	Atomic Force Microscopy
FT-IR	Fourier Transform Infrared Spectroscopy
GO	Graphene Oxide
NPs	Nanoparticles
PVP	Polyvinylpyrrolidone
PVP-GO	Polyvinylpyrrolidone Added with Graphene Oxide
RT	Room Temperature
SEM	Scanning Electron Microscopy

Acknowledgements

First and foremost, I owe my deepest gratitude to my principal supervisor Professor Nunzio Motta for his valuable guidance throughout my research journey. I thank him for his time, patience, and financial support (Supervisory Scholarship), which helped me to piece all my testings to make this research project cohesive and meaningful. I would also like to thank my associate professor Cameron Brown who provided me with inspirations on the research topics and Professor Yin Xiao who kindly guided the future research focus.

This project was carried out under School of Chemistry and Physics at QUT. Acknowledgement goes to fee offsets provided by QUT as a permanent resident. Acknowledgment also goes to peers in Surface Science Group for their generous support, giving their time and essential help. I acknowledge the administrative support provided by the School of Chemistry and Physics. My appreciation also goes to the Central Analytical Research Facility (CARF) for providing cutting-edge scientific equipment and licensed software hosted by the Institute for the Future Environments (IFE) at QUT and CARF technicians (especially Yanan Xu) for providing comprehensive training sessions and extra learning resources.

Finally, and most importantly, I would like to thank my partner for his academic support and my parents for their spiritual support and understanding throughout this research. This journey would not have been possible if not for them and I dedicate this milestone to them.

Chapter 1: Introduction

In this chapter, Section 1.1 and 1.2 outline the background and context of the research, and its purposes. The following section (1.3) describes the significance and scope of the research and provides definitions of terms used. Finally, the last section (1.4) includes an outline of the remaining chapters of the thesis.

1.1 Background and Context

Polymer composites are a kind of high-performance and versatile compounds formed from the combination of different phases of materials, where the matrix is often a polymer[1]. Polymer nanocomposites fabricated by dispersing nanofillers or reinforcements have been found to have improved functional properties that are unachievable with a single material. The unique combination of the nanofillers' features such as size, amount, surface area that affects the polymer matrix, along with advanced characterisations have generated much research interest in the field of drug delivery, advanced material synthesis, aerospace components, etc[2, 3]. The properties of nanocomposite materials depend not only on the properties of their individual components, but also on their interactions, thus it is necessary to explore the relationship between nanofillers and the polymer matrix and to understand the mechanism of which nanofillers change the functional properties of the composite.

Molecular modelling via polymeric nanocomposites is widely used to understand the complexity of intermolecular interactions attributed to specific properties of a natural material. Termonia developed a microscopic model of the spider silk elasticity using β-pleated sheets and polyethylene to integrate the information known about the structure of the silk fibre and demonstrate the role of

crystallites which act as multifunctional cross-links and create inside the amorphous regions a thin layer with modulus higher than in the bulk[4]. The role of the crystallites in spider silk is found to be similar to that speculated for carbon black in synthesised elastomers[4]. Inspired by this modelling, graphene based nanoplatelets have been considered as alternative fillers due to their unique physical and chemical properties. The two-dimensional (2D) allotropic structure of graphene based nanoplatelets such as graphene oxide (GO) allows to apply them in various biological fields, thanks to their good mechanical properties[5]. Polyvinylpyrrolidone (PVP) has been used as polymer matrix due to its excellent wetting and mechanical properties.

The knowledge of the fundamental structure-property relation of how nanoparticles (NPs) impact on the mechanical properties of the polymeric material by varying (1) the particle size and (2) concentration is expected to lead to more precise structural organisation and functional optimisation in order to produce advanced materials for further applications.

1.2 Aims and Objectives

This project aims to investigate change in mechanical properties of bulk material and nanofibers of PVP polymer by adding GO platelets. The role of GO platelets is investigated by varying (1) platelet size and (2) concentration in weight. This is expected to provide critical data to understand the underlying mechanism of interaction between platelets and polymer matrix.

The objectives to be achieved are as following:

(1) To prepare GO platelets with different size via ultrasonication and centrifugation techniques

(2) To optimise the parameters of ultrasonication including sonication time and temperature

(3) To determine the concentration of GO supernatants via UV-Vis spectra

(4) To optimise the electrospinning parameters including polymer solution concentration, collection distance, applied voltage and feed rate, to produce polymeric nanofibers of desired size

(5) To investigate the mechanical properties of bulk material and nanofibers after GO is added

1.3 Significance and Scope

Most of the present literature focus on how nanofillers change the mechanical properties of the composite without attempting to understand the fundamental mechanisms[6]. From a theoretical standpoint, little progress has been made regarding the understanding of structure-property relationships in polymeric composite in form of both bulk material and nanofibers. A semi-crystalline polymer resembles most synthetic fibres where the origin of its exceptional functional properties remains obscure, which also leaves a research gap. In this research project, a simple polymeric system has been designed where the polymeric matrix is PVP and fillers are GO platelets. This work is expected to open up a new avenue to understand how nanoparticles play a role in changing mechanical properties of polymeric matrix in nanofibers. Due to the distinctive structural characteristics of GO, there would be some interactions expected in a polymer matrix. It will be of interest to investigate how functional groups attached to the surface of GO will change the properties of the composite by varying the size and concentration of GO. These points have not been discussed and literature on this is very limited.

As for the scope of this work, we focus on the interaction between PVP polymer and GO platelets. The characterisation of GO is performed by using Atomic Force Microscopy (AFM). We assume that the concentration of GO is correctly present in the electrospun nanofibers because GO are well distributed in polymer solution and the amount of residue solution in the syringe involved in electrospinning process is neglectable. The study of mechanical properties including hardness, Young's modulus is carried out using nano-indenters.

1.4 Thesis Outline

Chapter 2 presents a comprehensive literature review to gather knowledge on PVP, GO and other relevant techniques utilised in this project. Chapter 3 recalls the methodology. The instruments and data processing involved in this project are also illustrated in Chapter 3. Chapter 4 analyses the characterisations of GO platelets with different size and different concentration. Chapter 5 focuses on the characterisations of electrospun PVP Polymer and its composites under different electrospinning parameters. Chapter 6 discusses the mechanical properties of prepared PVP bulk material and nanofibers. Chapter 7 is the conclusion of the project by chapter which also includes the limitations, implications for practice and future research directions.

Chapter 2: Literature Review

In this chapter, the literature review will be introduced on the following topics: Molecular Modelling of Spider Silk (Section 2.1); Polyvinylpyrrolidone (PVP) (Section 2.2); Graphene Oxide (GO) (Section 2.3); The Effect of Size and Concentration of Nanofillers (Section 2.4); The Effect of Ultrasonication Technique (Section 2.5); Electrospinning of Polymeric Materials (Section 2.6). Section 2.7 presents a summary of the literature and the implications of this project.

2.1 Studies of the Spider Silk Microscopic Structure

Spider silk has attracted human interest for decades due to its toughness and ductility[7]. Silk fibres are well known as materials for medical uses and recent developments have seen their potential in various important applications ranging from ligaments to nerve repair, and even considered for hypothetical artificial muscles[7, 8].

Spider fibres are primarily composed of proteins found in different groups of arthropods. The repetitive sequences often account for 90 % of the whole spider protein and are composed of short polypeptide stretches for 10 to 50 amino acids[9]. Each polypeptide repeat has distinct functional features, resulting in outstanding mechanical properties of a unique combination of toughness and elasticity compared to man-made chemical polymers[9]. The most well studies spider silk is the dragline of the major ampullate Spidroins (MaSp1 and MaSp2) from *Nephila clavipes* that are sensitive to sheer stress, drying and hydration[10]. The strongest spider dragline silks have been found as a hybrid structure comprising about 45 to 65% hard domains of beta sheet folds in a matrix of mixed helical conformer chains. Some studies describe

these regions to adopt amorphous rubber-like amorphous matrix, while others suggest formation of helical structure[11]. As polymeric fibres, they are a unique combination of being seemingly highly oriented but having a moderately high elastic modulus (about 10 GPa) which is essentially isotropic[8].

There are commonly two simplifying constraints, derived from the natural origin of the material and derived from the polymeric functionality of the material[12]. Silk structure can be reduced to that of ordered and disordered domains at the nano-meter scale due to the dominance of hydrogen bonding in determining the semi-crystalline morphology of the polymers. Fig 2.1 shows different types of silk morphology developed by scientists and biologists. Fig 2.1 (a) illustrates a hard domain in an amorphous matrix; Fig 2.1 (b) shows the a sketch of separate disordered chains, while Fig 2.1 (c) shows an extreme biological perspective composed of a single folded chain beta sheet crystal domain surrounded by helical structures[7].

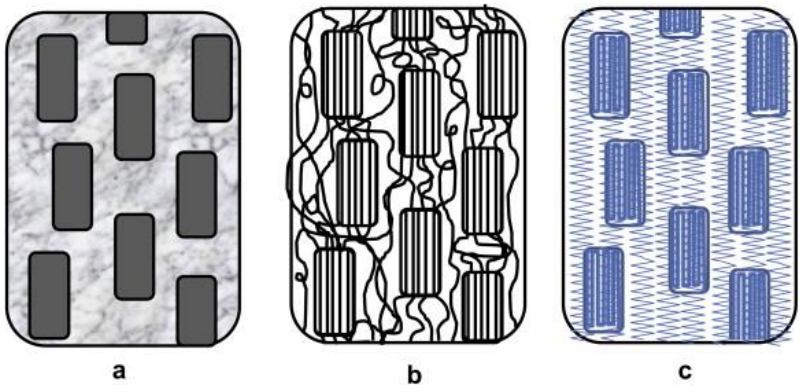

Figure 2. 1 (a) Hard crystal domains in an amorphous matrix, (b) A polymer sketch with separate chains converging into the crystal domains, (c) Folded beta sheets in a helical matrix (Adapted from reference [7])

Termonia was a pioneer in the study of spider silk structure via molecular modelling, using β-pleated sheets and polyethylene to integrate the information

known about the structure of the silk fibre[4]. The model demonstrates the role of crystallites as multifunctional cross-links inside an amorphous polymeric region; the study also found that the role of the crystallites in spider silk is similar to that speculated for carbon black in synthesised elastomers[4].

2.2 Polyvinylpyrrolidone (PVP)

2.2.1 Introduction of PVP

PVP is a hygroscopic, amorphous, synthetic polymer consisting of linear 1-vinyl-2-pyrrolidinone groups (Figure 2.2)[13]. It can be prepared by free-radical polymerisation from its monomer N-vinylpyrrolidone in the presence of azobisisobutyronitrile (AIBN) as an initiator. Different degrees of polymerisation of PVP resulted in polymers of various molecular weights, which are distinguished by their viscosity in aqueous solution relative to that of water and expressed by a K-value ranging from 10 to 120, such as PVP-K12 (3,100-5,700 g/mol), PVP-K17 (7900–10,800 g/mol), PVP-K25 (23,000–32,000 g/mol), PVP-K30 (35,000–51,000 g/mol), and PVP-K90 (900,000–1,300,000 g/mol)[13].

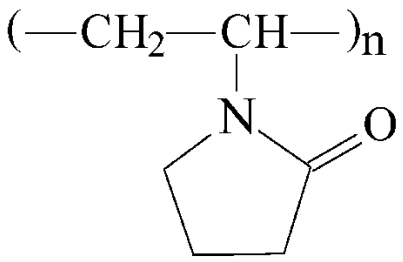

Figure 2. 2 Structural formula of PVP

There are two forms of PVP dependent on the polymerisation conditions: (1) Soluble PVP, also named as povidone and (2) insoluble PVP (crospovidone)[14]. PVP is a highly polar, amphiphilic polymer which is compatible with a variety of resins

and electrolytes. Commercialised soluble PVP is a light flasky powder that readily absorbs up to 40% of water by its weight[15]. It also has excellent solubility in solvents of different polarities and good binding properties. In solution, it exhibits excellent stabilising effect, wetting properties and readily forms films[16]. PVP has unique physical and chemical features, including being chemically inert, temperature-resistant, and pH-stable[15].

2.2.2 Applications of PVP Based on its Properties

2.2.2.1 Biocompatibility

Due to the biocompatibility and low toxicity, PVP has been widely used in the food sector, cosmetics, biological-based materials, and pharmaceutical industries[16, 17]. PVP was previously used as a plasma volume expander for trauma victims during the Second World War[16]. Recently, it has been used as a binder in pharmaceutical tablets for quick drug release[18]. Also, PVP provides stability to tablet formation and can be combined with other reagents to form gelatin capsules of insoluble drugs[15]. Many germicidal products with PVP added have exhibited reduced toxicity and intensity of skin reactions while maintaining its germicidal activities[15]. PVP is also widely used in eyes drops, contact lenses and their package solutions which acts as a lubricant to reduce friction due to its excellent wetting properties[14, 18].

2.2.2.2 Molding Agent

PVP has been used to prepare and shape controlled noble metal nanoparticles, which can avoid the aggregation of particles and uphold an identical colloid dispersion as a stabilising agent[15]. Zhang et al used PVP as stabilising agent in inorganic solar cells and achieved a high-performance device[19]. It is also used as a shape-control agent, which supports the growth onto precise faces while preventing

the growth onto others, widely applied in the polyol synthesis of nanoparticles as catalysts and substrates for chemical sensing[20].

2.2.2.3 Spinnability

Pure PVP and its polylactide blends were first used for electrospinning to fabricate fibres in 2001 and has been widely used to manufacture fibres from different materials using electrospinning process due to its spinnability and fibre extraction[21]. Furthermore, conductive polymers, biopolymers, and other organic/inorganic compounds were used as a filler in the PVP polymer matrix and directly blended with the PVP solution to obtain PVP-based electrospun fibres[21].

2.3 Graphene Oxide (GO)

Graphene and its chemical derivatives have drawn great research interest due to their excellent thermal and electrical conductivity, biocompatibility, unique optical behaviours, excellent mechanical properties, extreme chemical stability, and a large surface area[22, 23]. These properties arise from two-dimensional (2D) crystallographic nature of graphene, which is a one-atom thick sheet of sp^2 hybridised orbitals in a tightly packed honeycomb lattice[12, 24]. Each carbon atom is comprised of three σ-bonds and an out-of-plane π-bond that bind with neighbouring atoms. Furthermore, graphene sheets can be altered to graphene-based materials such as single and multi-layered graphene, GO and reduced GO via chemical and physical modifications[23]. GO contains a single layer of sp^2 carbon atoms with hydroxyl and epoxy functional groups on the surface, and the carboxyl groups at the edges (Fig 2.3). These functional groups offer active sites for further reactions and GO has been reported to show hydrophilic characteristics and good biocompatibility[25, 26]. This offers potential

in biomedical research such as bioelectronics, imaging, drug delivery and tissue engineering[23].

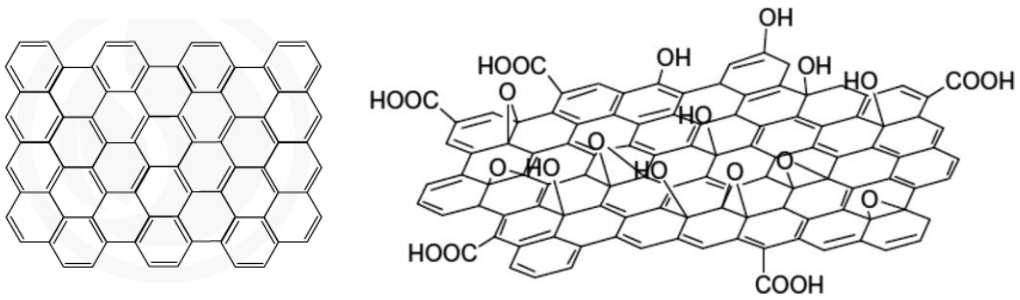

Figure 2. 3 Left-Graphene structure, Right-Proposed graphene oxide structure [27]

The incorporation of graphene based materials into polymeric chains can enhance the mechanical properties, heavily relying on the distribution of the graphene with the polymer matrix and interfacial bonding between the graphene and the host matrix[6]. The distribution of the graphene within the polymer is significantly affected by the polarity of the polymeric backbone where a hydrophilic polymer may cause the aggregation of the graphene layers due to the interactions between the graphene layers and hydrophilic polymer chains[28]. Naturally hydrophobic graphene disperses within a hydrophobic polymer matrix through π-π stacking[28]. The weak interactions of graphene with the host matrix have made the low stress transfer between the immiscible components, therefore often resulting in low tensile and elongation characteristics[28]. In contrast, GO sheets having oxygen functional groups heavily bonded to the surface, are more compatible with organic polymers. Also, GO achieves molecular dispersion due to the interactions of oxygen containing functional groups towards the hydrophilic based polymer chains[29]. Despite dispersion, hydrogen bonds could enhance the interfacial adhesion and the mechanical performance of the composite[30]. For biomedical applications, a strong bond between fibres and the matrix is highly desirable to ensure stability of composite materials in *in vivo* environment[31].

2.4 The Effect of Size and Concentration of Nanofillers

Elastomeric composite with nanosized fillers was first used in 1959 and a proper research started in 1990 when Toyota attempted to exfoliate clay nanofillers in nylon, which demonstrated significant improvement in a wide range of mechanical properties of the material in the fabrication of automobile tyres[32].

2.4.1 Size Effect

Composite properties are influenced by fillers to a large extent. The size of filler materials has a profound effect on the resulting properties of composites[33]. This is because surface interactions with the matric, adhesion, particle motion, dispersion and bonding all depend on the size of fillers. When the size is down to nanoscale, effects such as quantum confinement, quantisation of energy, electromagnetic forces become important[33]. This gives rise to increased intermolecular bonding, hydrogen bonding, van der Waals bonding, surface energy, and so on[33]. Some studies also showed the change of composite performance due to the geometry (aspect ratio and orientation) of added nanofillers[2]. It has been acknowledged that the reinforcement efficiency increases with an increasing aspect ratio[34]. Similarly, with a high aspect ratio (length over diameter), fillers such as monolayered GO sheets reinforced composite material displays produce enhanced mechanical properties in directions parallel to the reinforcement[34].

2.4.2 Concentration Effect

There are studies showing the effect of filler concentration in polymer composites[3]. A low filler concentration usually suggests a weakly connected network between nanoplatelets and matrix due to a larger distance among nanoplatelets[3]. This

network often has small connectivity and could easily separate into non-percolating clusters if the physical bonds between polymer and platelet break up[3]. This makes a higher filler concentration beneficial for some composites due to a decreased distance between platelets and increased connectivity between polymer and platelets. Some studies suggest that a high filler concentration enables a high crosslinking density which provides a strong interconnection in the system so that the breaking of single physical bonds has limited effects on the overall network[3].

However, studies show the negative effects of a loading levels higher than percolation threshold on mechanical properties due to aggregation of nanofiller in the polymer matrix[35]. This results in a decrease in effective active surface area of the filler phase and a weaker interfacial adhension[35]. This suggested the importance of determine a critical filler concentration to achieve the desired performance, depending on the properties of fillers and polymer matrix.

2.5 Ultrasonication Techniques

Ultrasonication refers to the irradiation of a liquid sample with ultrasonic waves that cause the periodical compression and rarefaction when propagating through the medium, resulting in agitation[36]. It is a versatile method to disperse nanofillers in solution by the high energy that drives the separation of agglomerates of nanofillers since the high-frequency waves create higher energy compared to the interaction energy between nanofillers in agglomerates[33]. These small bundles of nanofillers progressively exfoliate into smaller size with extended sonication time[33]. Several studies also show the effectiveness of exfoliation, especially for layered nanosheets such as GO in a low-viscosity solvent or solutions via ultrasonication[33].

There are multiple parameters that control the effectiveness of agitation and exfoliation, such as sonication time, power and temperature[37]. The sonication power usually ranges from 100 W to 1500 W. The choice of sonication power should be based on the types of nanofiller and their dispersion states. A high power may not damage nanofillers such as nanospheres but can lead to serious fragmentation of 1D nanofillers such as nanosheets, resulting in a larger aspect ratio as discussed above. Sonication time also plays a role in fragmentation. Studies show the higher level of fragmentation of nanosheets with an increase in sonication time[33]. However, sonicating for too long could lead to an increased number of defects, which could be deleterious to the mechanical properties of nanocomposites[33]. Additionally, some studies also show the occurrence of reagglomeration after extended period of sonication[33]. Sonication temperature is another factor[38]. On one hand, high temperatures can help to disrupt solvent-solute interactions, involving H-bonding and faster diffusion. On the other hand, a too high temperature decreases the efficiency of ultrasonic effects caused by the natural bubbles of vapour from the solvent[39].

Nevertheless, bath sonication operated in intervals with controlled temperature can be effective and efficient to stop agglomeration and promote dispersion and exfoliation of nanofillers in low-viscosity solutions[33].

2.6 Electrospinning of Polymeric Materials

2.6.1 History and Background of Electrospinning

The electrostatic attraction of a liquid was first introduced in 1600 by William Gilbert after he conducted a series of experiments using an electrically charged piece of amber[40]. He observed that the water droplet attained a conical profile in the proximity of charged amber and it were drawn by means of air rushing along and

deformed into what would eventually become known as Taylor cone[41]. His experiment was the foundation for electrospinning and electrospraying[41]. It was first patented in 1934 by Anton Formhals for the fabrication of textile yarns[42]. There is evolution of electrospinning techniques occurring over the time and in the early 1990s, electrospinning became popular. Several research groups, notably Reneker and his co-workers have made big progress using organic polymer melts to produce electrospun nanofibers present with various morphologies, sizes and applications[43]. Deitzel et al, and Shafiei et al have developed a method to control the motion of charged jet using an electostatic ring, giving a better control of deposition area on sensing platforms[44, 45]. Most recently, co-electrospinning techniques have been extensively developed to produce electrospun fibres with hollow, multichannel, porous and thin-wall assembled structures that can be applied in various fields[46]. Besides the controllable morphology for fibres, the ability to control the arrangement of fibres becomes critical to achieve desired properties, particularly for mechanical enhancement and tissue engineering, as a support for tissue generation [42, 46].

2.6.2 Basic Setup and Principles

Electrospinning is one of the most simple, robust, and cost-effective techniques to produce polymer and polymeric composite fibres with a diameter size range of nanometres up to a few micrometres[47]. A high voltage power source is usually required enabling the production of fine fibres from a polymer solution or polymer melt. A typical electrospinning setup (Fig 2.4) for polymer solution consists of components including (1) a syringe containing the solution or melt for electrospinning, (2) a capillary tube used as a first electrode (e.g. a metallic needle with a blunt tip), (3) a syringe pump that controls the feed rate, (4) a direct current

high voltage power source and (5) a grounded collection plate, used as a second electrode[46].

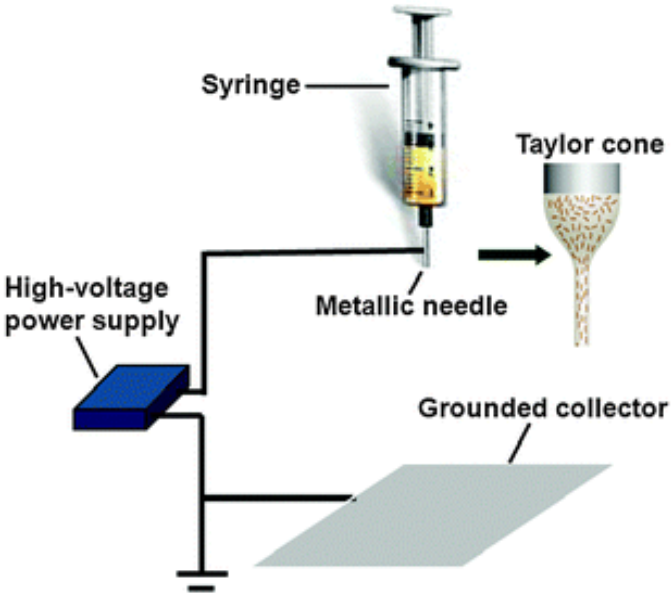

Figure 2. 4 Schematic representation of laboratory setup for electrospinning (Adapted from reference [46])

The electrospinning process is based on the electrostatic effect on a high viscosity fluid, in which a hemispherical droplet of the polymer solution is subjected to an electric force and suspended at the end of the needle tip. Electric charges accumulate at the droplet and tend to be elongated to form a cone shape, named as Taylor cone, where the surface tension reduces the surface area. When the charged repulsive expansion exceeds the contractions of surface tension, a charged jet of solution is ejected from the Talyor cone and travels towards the target surface, usually chaotically. The jet follows a path which begins with a linear segment and accelerates as the Coulomb forces pull it towards the collector against the surface tension and viscoelastic forces. Then the linear segment of the jet becomes unstable due to the presence of Coulomb repulsion of the charge and elongates in the electrical field and bends and grows into a coil of increasing diameter. The process is

repeated until the elongation stops by solidification of the thin jet when solvent evaporates. The resultant solidified fibres that reach the collector are usually in the form of nonwoven mesh[42].

In general, soluble polymers processed to nanofibers by electrospinning involve a set of parameters governing the electrospinning process. This includes the properties of the polymer itself (such as molecular weight, solubility, melting point, and glass-transition temperature), the properties of the polymer solution (such as viscosity, concentration, conductivity, surface tension, solvent effects, and temperature), and parameters of electrospinning process (electric potential, collection distance between needle and collector, collector plate, feed rate, and relative humidity)[46]. Each parameter significantly influences the morphology and size of electrospun fibres, which needs proper manipulation to obtain the desired product. Utkarsh et al and other researchers have summarised five important parameters and their effects on fibre diameter and morphology for current electrospinning practice, stating that polymer concentration and voltage applied have more significant effects on fibre morphology compared to the feed rate, the collection distance and collector rotation speed [21, 48-50]. It is also worth noting that to achieve uniform beadless fibres, the viscoelastic force of solution should be sufficient to break the polymer jet with higher coulombic stress that influences the jet elongation[21]. This could be achieved by increasing the concentration, taking care of not bypassing the limit beyond which the solution could restrict the continuous flow and block the needle. The effects of the main parameters on the resulting fibre morphology have been summarised in Table 2.1.

Table 2. 1 The effect of electrospinning parameters[49]

	Change	Fibre diameter	Fibre shape
Viscosity (Concentration) of polymer solution[50]	Increased	Increased	Reduced bead formation[48]
Collection distance	Increased	Decreased	n.a.
Electric potential	Increased	Decreased	affected
Feed rate	Increased	Increased	affected

2.6.3 Electrospun Fibres Incorporated with Nanoparticles (NPs)

Recently, there is much research attention and interest in the development of electrospun fibres incorporated with functional NPs, in order to improve the performance of electrospun fibres or films depending on the type of polymer and the NPs added. Direct fabrication is one of the most straightforward strategies to produce composite electrospun fibres that has been widely used[46]. There are different kinds of NPs that have been uniformly distributed in polymer solution and directly electrospun, which can be divided into four main classifications including[46, 51]

1. Zero-dimension (0D) NPs-quantum dots or zero-dimensional particles
    - Metal (Ag, Au), metal oxide (SiO_2, TiO_2, MgO, ZnO and ZrO_2), quantum dots and polymer spheres (microgels)
2. One-dimension (1D) NPs-wires
    - Organic nanochains, inorganics (Au nanorods and nanowires)
3. 2D NPs-layered particles or sheets
    - Clay nanosheets, GO nanosheets
4. other organic or biomolecules

2.6.4 Electrospun Fibres Incorporated with NPs for Mechanical Enhancement

The research on mechanical enhancement of composite nanofibers prepared by electrospinning usually focused on two types: (1) to reinforce the composite

nanofibre itself and (2) to reinforce substrate material, i.e. nanofiber reinforced composite substrate[52]. The electrospun nanofibers have been found to be promising materials since they tend to have better mechanical properties due to the formation of self-organised structures in the electrospinning process[46].

It is known that decreasing the diameter of fibres can increase the strength although at expense of their toughness. However, recent research has reported both strength and toughness of PAN electrospun fibres increase when the diameter of fibres was less than 250 nm[53]. Moreover, by adding carbon nanotubes to different polymers such as PAN, PU, PS and PLA, etc, the mechanical property of the composite fibres could be greatly enhanced[54, 55]. Carbon materials with 2D structure such as graphene based nanoplatelets were also proven to enhance the mechanical properties of electrospun fibres[52, 56].

2.7 Summary and Implications: The Knowledge Gap

This literature review has introduced the existing molecular modelling of spider silk which gives the inspirations for this work. The properties of polymer PVP and nanofillers GO used in this project have also been discussed in terms of their structure and characteristic properties. The biocompatibility and electrospinnability of polymer PVP enable the fabrications of nanofibers possible, together with its compatibility of the addition of nanofillers. The extensive properties of GO platelets are expected to change the overall performance of the polymer matrix.

The effect of size and concentration of nanofillers in nanocomposite, and the effect of ultrasonication in solution preparation have also been discussed in terms of the existing research, which provides the guideline of the desired range of GO platelets and solution preparation. The review extensively discusses electrospinning

of polymeric material from its history to the effect of electrospinning parameters, which provides indications of tuning different parameters for an optimal fabrication of electrospun nanofibers in terms of the diameter and the morphology.

The review highlights that in-depth studies of structure-property relation of PVP and GO mixtures by varying the concentration and the size of GO platelets have not yet been conducted. The present work can potentially give insights to understand the fundamentals of polymeric composites as bulk materials or nanofibers. Additionally, the mechanical testings of polymeric nanofibers are full of challenges and worth investigating.

Chapter 3: Research Design

This chapter outlines the design and methodology of the research to achieve aims and objectives stated in Section 1.2. Section 3.1 discusses the methodology used in the project, the stages by which the methodology is implemented and the research design. Section 3.2 lists all the instruments used and justifies their use for structural characterisations and measurement of mechanical properties. Section 3.3 discusses how the data are processed and analysed.

3.1 Methodology and Research Design

The methodology is organised in relation to research objectives and problems. The stages of the research project are shown as following:

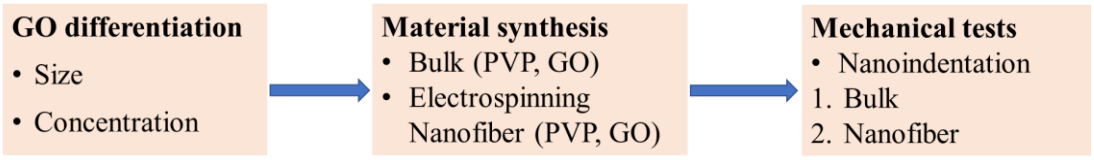

3.1.1 GO Differentiation (Size and Concentration)

Pristine GO platelets (4 mg/mL concentration, Graphenea) were prepared into different sizes and concentrations.

GO (5 mL) was dispersed into DI water (20 mL) and sonicated for 1, 2, 3, 4 ,5 and 6 hours with an iced bath. The ice bath was changed every 30 minutes to ensure the dispersion stayed in the temperature range 0 - 4 °C. The resultant GO dispersions were further diluted in DI water (50 mL) and centrifuged at speed 3,500 r.p.m (Fig 3.1). The supernatant of the six dispersions was carefully collected and named as

GO-1hr, GO-2hr, GO-3hr, GO-4hr, GO-5hr, and GO-6hr.

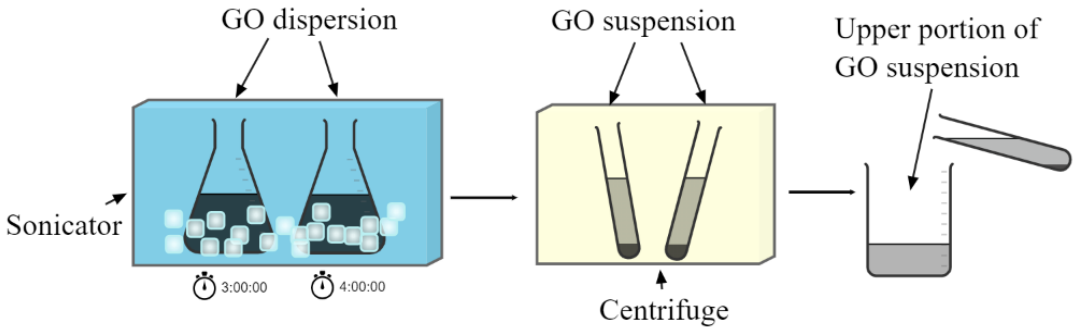

Figure 3. 1 Experimental procedures to obtain GO suspensions.

The six supernatant solutions were diluted in DI water, drop cast on a mica substrate and dried overnight at 70° C. They were analysed using atomic force microscope (AFM) and only two supernatant solutions were selected for further experimental procedures due to their proper size and distribution that matched the research interest (GO- 3hr and GO-4hr).

These two solutions were further analysed by UV-Vis Spectrometer for concentration identification. Three standard GO solutions (0.02 mg/mL, 0.04 mg/mL, 0.08 mg/mL) were prepared by diluting pristine GO solution in DI water and sonicating in water bath for 15 minutes. The maximum peak was identified as 230.4 nm using UV-Vis Spectrometer. Quartz cuvettes with a 10 mm optical path were used. According to Beer-Lambert Law which can be written as[57]

$$A = \varepsilon bc$$

where A is absorbance, ε is the molar absorptivity (L mol $^{-1}$cm^{-1}), b is the path length of the sample, expressed in cm and c is the concentration of the solution, the absorbance of the maximum peak is directly proportional to the concentration of the solution. A standard curve was drawn and defined as $A = 48.4554c + 0.0434$. The

absorbance of GO-3hr and GO-4hr was identified and plotted in the standard curve, with their concentrations calculated.

3.1.2 Synthesis of Bulk Material

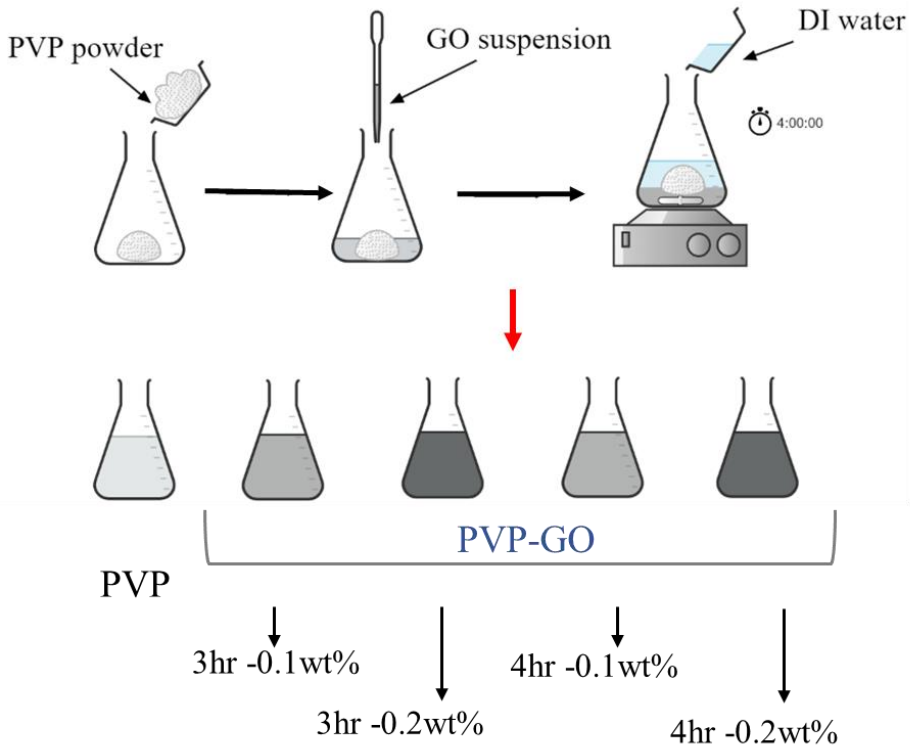

Figure 3. 2 Experimental procedures of synthesising bulk materials

PVP powder (Mw 1,300,000 g/mol, 100% purity from Sigma-Aldrich, USA) was chosen due to its proper viscosity for further experimental procedures (electrospinning process). Pure PVP gel (20 wt. %) was prepared by sol gel method, placing PVP powder (4 g) in a volumetric flask (50 mL) with DI water (16 g) added. The mixture was stirred using a magnetic stirrer bar at 350 rpm for 4 hours at room temperature (RT) until a colourless clear viscous solution was obtained and was stood overnight for air bubbles to escape. Using the method above, GO-3hr and GO-4hr were added in a mass percentage of 0.1% and 0.2%, synthesising four different composite gels (Fig 3.2). Their synthesis parameters are shown in Table 3.1 where

each sample is identified by the sonication time and the GO dispersion wt.%. The resultant polymer solutions were ultrasonicated for 15 minutes to ensure even dispersion of GO platelets in PVP solution.

Table 3. 1 Abbreviations of obtained PVP-GO composite gel

GO platelets	GO-3hr		GO-4hr	
Weight %	0.1	0.2	0.1	0.2
Polymer	PVP			
Composite	GO-3hr-0.1wt%	GO-3hr-0.2wt%	GO-4hr-0.1wt%	GO-4hr-0.2wt%

3.1.2 Synthesis of Nanofibers via Electrospinning

3.1.2.1 Electrospinning Setup

The basic principle of electrospinning has already been discussed in the literature review (Section 2.5). This section includes the electrospinning system design and steps of nanofiber fabrication. A horizontal electrospinning setup was designed at QUT and fabricated from Perspex. The in-lab electrospinning setup includes: (1) Safety box (acrylic material), (2) High voltage source (20 kV, 0.5 mA, PS375 Stanford research systems), (3) Syringe pump (NE-1000 New Era Pump Systems, Inc), (4) Insulation wooden board, (5) Plastic syringe (1 mL) with a blunt metal needle (21 G) (Fig 3.3).

A safety box made of acrylic material was used to avoid any potential electrocution under a high voltage working condition and avoid the exposure to evaporated solvents generated during the procedure. The front door was sealed with Teflon tape to prevent any leakage. The high voltage power supply can supply up to 20 kV DC and draws a current of 0.5 mA. The syringe pump was used for

continuous infusion of electrospinning solution via the blunt needle, which has a feed rate from 0.73 µL/hr to 2100 mL/hr (1 mL syringe) (Fig 3.3).

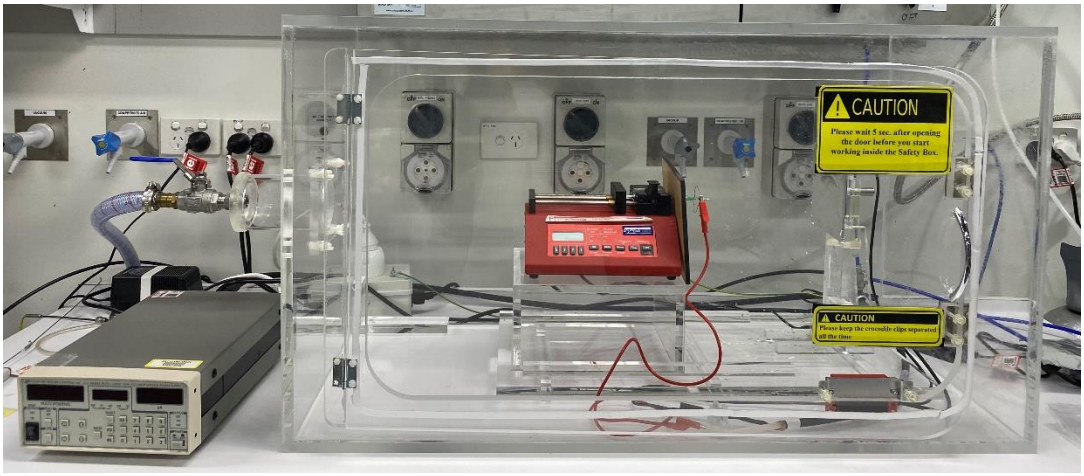

Figure 3. 3 Photo of electrospinning setup used in this work

The design of the electrospinning setup is shown in Fig 3.4, where the working distance can be controlled by moving syringe pump stand linearly between 1 cm to 20 cm. An insulation board is placed through the needle and the power supply is clipped onto the tip of the needle. The metal collector can move upwards and downwards.

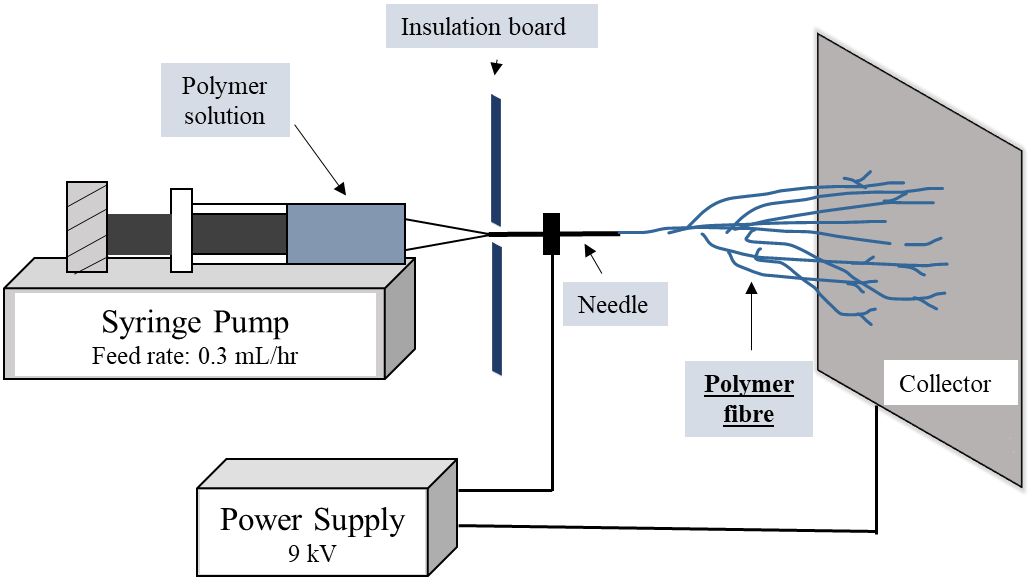

Figure 3. 4 Design of our electrospinning setup

3.1.2.2 Synthesis of Nanofibers via Electrospinning

The electrospinning gels were loaded into a 1 mL syringe with 21 G blunt stainless-steel needle. The electrospinning parameters were optimised to obtain beadles and straight fibres with a required diameter range. It was found that the optimal parameters are 9 kV for the high voltage, a feed rate of 0.3 mL/hr and a collection distance of 8 cm. The electrospun nanofibers were collected on a piece of aluminium foil wrapped around the metal collector.

3.2 Instruments and Material Characterisations

Several surface characterisation techniques were used for pristine and treated GO. These techniques were used to investigate the thickness and size of the GO platelets.

3.2.1 Atomic Force Microscope (AFM)

AFM is an instrument used for mapping the atomic-scale topography of a surface by means of the repulsive electronic forces between the surface experienced by a tip moving above the surface that causes the deflection of cantilever[58]. Deflection of the cantilever is commonly measured by the change in position of a laser beam reflected from the cantilever onto a photodetector[59]. A larger distance between the cantilever and the photodetector allows a smaller deflection to be measured.

Fig 3.4 shows the force received by a tip under corresponding scanning modes. In contact mode, a tip remains in contact with the sample and the static deflection of the cantilever is measured as the tip moves along the surface, which usually provides a high-resolution image. However, contact mode could result in damage to the tip

or/and deformation of soft samples. In non-contact and tapping (or semi-contact) mode, AFM measures the dynamic oscillation of the cantilever where the cantilever is oscillated at its resonant frequency and distance from the surface is measured by changes in the oscillation amplitude or frequency when a tip traces the surface. A change in the interaction due to a higher force causes oscillation damping and resonant frequency change. The instrument used in this work is a Bruker Icon Dimension equipped with the PeakForce™ tapping mode. PeakForce™ tapping mode avoids the lateral force on the tip by intermittently contacting the surface. It operates at frequencies well below the cantilever resonance, thus avoiding the filtering effect and dynamics of a resonating system[60]. The piezo is modulated up and down by a sin wave, generating force curves at every point. Based on the PeakForce™ Tapping mechanism, ScanAsyst ™ imaging mode provides fundamental advantages over contact and non-contact mode since the tip moves perpendicularly to the sample surface, thus reducing horizontal forces that protect the tip or/and sample and reduces the effect of the contamination layer on the acquired image[61].

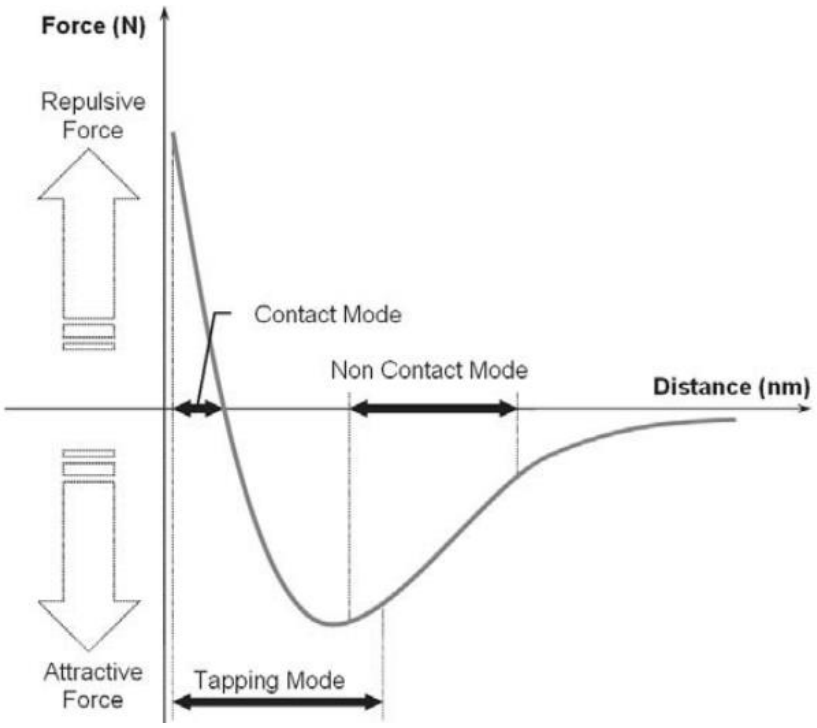

Figure 3. 5 Force-distance curve showing different modes of AFM (Adapted from reference[62])

Images acquired in ScanAsyst™ imaging mode used cantilevers with a silicon tip curvature radius of 2 nm, a resonance frequency in the range of 45 and 95 KHz, and spring constant of 0.4 N/m. The measurements were carried out under ambient conditions (~50% Relative Humidity and 23°). The GO platelets were drop-casted on a mica substrate. AFM images were further analysed using Gwyddion and Nanoscope software to calculate the thickness and surface size of GO platelets.

3.2.2 Scanning Electron Microscopy (SEM)

Scanning electron microscopy (SEM) is an observation method used to evaluate the micro-morphology of sample surface by receiving, magnifying, and displaying the physical signal of the sample excited by scanning a high-energy electron beam [63]. The detailed working principle is outside the scope of this study. The surface morphology of electrospun nanofibers is investigated using secondary

electron (SE) of SEM. The obtained images were further processed using Image J software to calculate the mean fibre diameter and distribution from 50 measurements on different fibres for each SEM image.

Electrospinning parameters were optimised based on the SEM images of nanofibers showing a minimum number of beads and a fibre diameter approximately 300 nm. A small amount of electrospun nanofibers was transferred on a carbon tape and coated with a 10 nm gold coating on top to improve conductivity and prevent charging. A low acceleration voltage (5 kV) with low current was selected for polymeric nanofibers to prevent them from melting. A working distance of 8 mm was used for SE detector.

3.2.3 Raman Spectroscopy

Raman is a molecular spectroscopic technique that provides detailed information about chemical structure, phase and polymorphy, crystallinity and molecular interactions based on the light scattering with the chemical bonds within a material[64]. In Raman, the light is inelastically scattered by the sample due to excitation or de-excitation of molecular vibrational states, and the emitted photon has an energy different from the incident photon. In Stokes scattering, the molecule is excited from a vibrational energy state to a virtual state, relaxing into a higher vibrational energy state: the emitted photon has energy equal to the incident photon energy minus the difference in the vibrational energy of the states. In anti-Stokes scattering, the process start from an excited vibrational state and ends into a lower energy vibrational state: the emitted photon has an energy equal to the incident photon energy plus the vibrational energy of the state (Fig 3.6)[64].

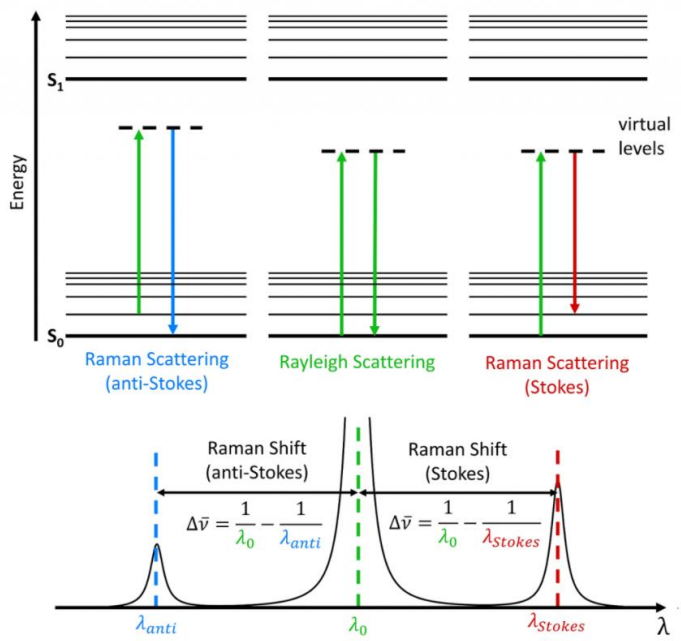

Figure 3. 6 Jablonski diagram showing the origin of Rayleigh, Stokes, and Anti-Stokes Raman Scatter (Adapted from Reference[64])

The vibrational states measured by a Raman spectrometer are characteristic of the bonding structures between atoms. GO have very intense Raman features, like graphene, which have been studied in depth, providing very clear identification of the bonds present and of the quality of the material[65]. In this project, a Reinshaw inVia Raman microscope with a He-Ne laser (λ=532 nm) was used as excitation source. The laser was focused using a 50 × objective lens which gives a spot size of 1 μm, and the power was limited to reduce local heating of the samples. The Raman spectra featured graphene-based materials regarding their number of layers, doping and strain by several peaks showing the intensity and wavelength position of scattered light which correspond to molecular bond vibration. The G band corresponds to a E2g in-plane vibration of the C-C bonds, and D and 2D bands arise from the breathing mode of the graphene carbon rings[66]. The D band is associated

with disorder, dopants or functionalised atoms and edges in the graphene layers which is commonly seen in GO.

3.2.4 Fourier Transform Infrared Spectrometer (FT-IR)

FT-IT Spectrometer is a device for qualitative and quantitative analysis of sample composition, especially functional groups by detecting the absorption or emission from samples, which correspond to the bonds present in the materials[67]. This study mainly used FT-IR (Nicolet iS50 FTIR, ThermoFisher Scientific, USA) to detect the functional groups present in the pristine and treated graphene oxide platelets. The samples were heated on evaporation dishes in a vacuum oven overnight at 80° before measurements. The spectra were collected in the range 400-4000 cm^{-1}.

3.2.5 Nanoindentation

A nano-indenter controls the continuous change of the load to measure the indentation depth in real time, to measure the hardness and Young's Modulus of materials. The test results are calculated by the curve of force and indentation depth. In this project, the mechanical properties of bulk material and nanofibers were investigated using a Hysitron TI 950 triboindenter (Bruker Corporation, USA) with a displacement resolution of 0.04 nm and a load resolution of 1 nN. Various nanoindentation tests were carried out to study different aspects of mechanical properties of the material. To clearly illustrate the testing method used, detailed experimental setups are discussed as follows.

3.2.5.1 Indenter Types

The Berkovich indenter was used in the indentation studies of bulk material when they were dried to film, with the advantage that the edge of the pyramid is more easily constructed to meet a single point[68]. The face angle of the Berkovich indenter is 65.27° and the projected area of contact is $A = 24.5\,h^2$; A conical indenter was used to perform three-point bending tests in section 6.2.1 for nanofibers with the advantage of possessing axial symmetry, and the semi-angle for an equivalent conical indenter is 70.3°[68].

3.2.5.2 Measurement of Elastic Modulus and Hardness

In the indentation process, both load and displacement are recorded continuously in real-time. The size of contact area at full load is estimated from the depth of penetration with the known geometry of the indenter. An indentation cycle consists of loading and unloading process. In loading, material may deform elastically first followed by plastic deformation or fracture. If a plastic deformation occurs, a residual impression is left on the sample surface upon unloading[68]. The recorded Force-displacement curves enable the determination of both elastic modulus E and hardness H of a material[68]. In depth-sensing indentation techniques, the elastic modulus of the sample can be determined from the slope of the unloading of the load-displacement response. Ideally, the indentation modulus has the same meaning as elastic modulus or Young's Modulus.

Given the contact between a flat, frictionless surface and a rigid sphere, Hertz theory stated[69]:

$$a^3 = \frac{3}{4}\frac{FR_0}{E^*} \qquad (1)$$

where a is the radius of the contact circle, F the indentation load, R_0 is the radius of the indenter tip, and E^* is reduced modulus. The expression of E^* includes the moduli of the indenter and the sample, given by[70]:

$$\frac{1}{E^*} = \frac{1-v^2}{E} + \frac{1-v'^2}{E'} \qquad (2)$$

where E and E' are the elastic moduli of the sample and the indenter tip respectively; v and v' are the Poisson's ratio of the sample and the indenter tip respectively.

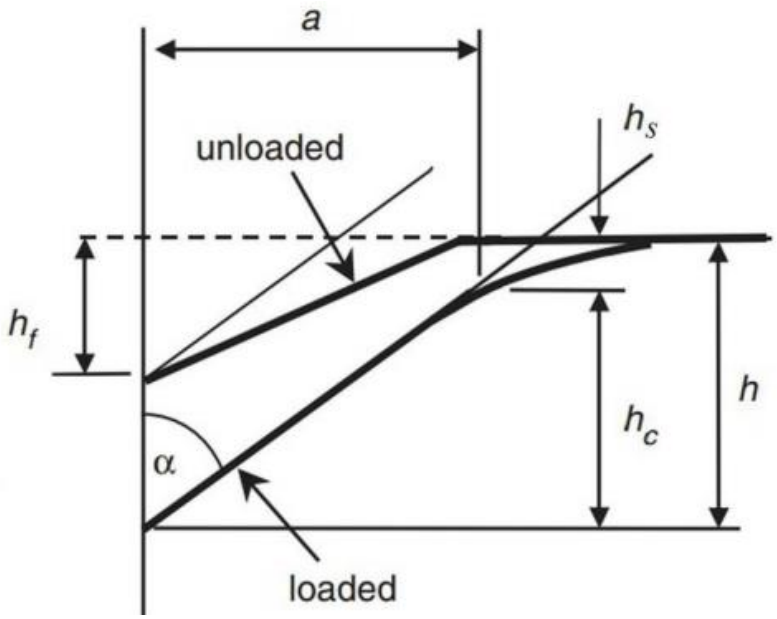

Figure 3. 7 The cross-sectional profile of a sample surface at full load for an elastic-plastic indentation where h is the indentation depth, h_c is the contact depth under full load; h_s is the depth of the uncontacted surface under indentation; a is the radius of the contact circle, α is the semi-angle of the cone; h_f is the final residual depth after full unload procedure (Adapted from reference[71]).

For a conical tip, the cross-sectional profile of a sample surface at full load is illustrated in Fig 3.7. The relation between the indentation load F and radius of the contact circle a can be written as:

$$F = \frac{\pi}{2} a^2 E^* cot\alpha \qquad (3)$$

where α is the semi-angle of the cone. The depth profile of the deformed surface within the area of contact h is[68]:

$$h = \left(\frac{\pi}{2} - \frac{r}{a}\right) a\cot\alpha \qquad r \leq a \qquad (4)$$

By substituting Equation (4) with $r = 0$ into Equation (3), we obtain:

$$F = \frac{2}{\pi} E^* \tan\alpha \; h^2 \qquad (5)$$

The derivative of the force with respect to the depth is referred as the contact stiffness:

$$\frac{d\,F}{d\,h} = 2[\frac{2}{\pi} E^* \tan\alpha]h \qquad (6)$$

From Equation (4) with r=0 and inserting into Equation (6), we obtain:

$$\frac{d\,F}{d\,h} = 2E^* a \qquad (7)$$

or equivalently:

$$E^* = \frac{1}{2}\frac{d\,F}{d\,h}\frac{\sqrt{\pi}}{\sqrt{A}} \quad (8)$$

where $S = dF/dh$ is often denoted as the contact stiffness of a material, which is the slope of the start of the unloading curve at the maximum load[72]. Equations (7) and (8) have been fundamental to show the elastic contact with any axis-symmetric indenter and a smooth profile and form the basis of analysis techniques where the contact stiffness is evaluated at the beginning of the unloading response. Reduced modulus E^* can be thus determined. Using Equation (2), the elastic modulus, or Young's modulus can be calculated.

Nanoindentation hardness is defined as the indentation load divided by the projected contact area of the indentation. It is the mean pressure that a material will

support under load. From the force-displacement curve, hardness can be obtained at the peak load as

$$H = \frac{P_{max}}{A}$$

where P_{max} is the peak load and A is the projected contact area.

For a conical indenter, the radius of the circle of contact is:

$$a = h_c \tan \alpha$$

where h_c is the depth of the circle of contact. And contact area A can be expressed as:

$$A = \pi a^2$$

In indentation testing, pyramidal indenters such as Berkovich indenter are usually treated as conical indenters with a cone angle that provides the same area to depth relationship as the actual indenter in question[68].

3.2.5.3 Three-point Bending Tests of Nanofibers

Three point bending flexural tests provide modulus of elasticity in bending of plastic materials, which require the load to be applied to the midsection of the test sample so that it is bent into a U or V shape with the outside surface experiencing tensile forces and the inside face experiencing compressive forces[73]. The applied force and the corresponding displacement at the midpoint are recorded and then used to calculate the Young's Modulus of the nanofiber. It involves clamping a nanofiber across a trench or hole by self-adhesion between the fibre and substrate or electron-beam induced deposition process[74].

The three-point beam bending theory for a beam with two fixed ends has been widely used to calculate the Young's modulus of a nanowire as follows[32]:

$$E = FL^3/(192dI)$$

Where F is the applied force at the midpoint, L is the suspended length of the wire, d is the displacement of the wire the midpoint and I is the section inertia moment of the fibre. For a circle section fibre, $I = \frac{\pi r^4}{4}$, where r is the radius of the fibre. The equation is based on the following assumptions: (1) the two ends of the fibre are fixed (rigid constraint), (2) the suspended length of the fibre is much larger than the wire diameter, (3) the weight of the fibre is negligible and (4) the deflection of the fibre is very small. Among the above four assumptions, a perfect clamp for the rigid constraint is difficult to achieve[32]. A simply supported nanofiber without any constraint at the two ends however can be obtained by[73]

$$E = FL^3/(48dI)$$

which is four times higher than that of the fixed-end wire predicted by equation.

3.2.5.4 Initial Contact Stiffness of Nanofibers

A Berkovich nanoindentater tip was used to indent nanofibers on Fluorine-doped Tin oxide (FTO) glass to perform an indentation test. The peak nanoindentation depth was set as low as 80 nm, which is about 30% of the fibre diameter. It is generally accepted that the depth of indentation should never exceed 30% of the fibre diameter to avoid the substrate effect on the measurement of elastic modulus of nanofibers. However, due to the large strain gradients in small indentations, geometrically necessary dislocations occurred in most nanofibers and substrate effects therefore were mostly observed in measured nanofibers. Instead, the initial contact stiffness defined as the slope of the fit for lower portion of the loading curve was measured because it had minimal substrate effect to study the mechanical behaviour of the nanofibers. 30 nanofibers of each sample were studies.

3.3 Data Processing and Analysis

All data were collected from experimental devices and instruments as discussed above and recorded in both network disk and hard disk at QUT. All instruments were used with the permission of technicians and sufficient training sessions. The comparison between experimental data of each group follows the control variable method to ensure the independence of the factors of interest. Qualitative analysis by FT-IR showed the functional groups present in the pristine and treated graphene oxide platelets. The size distribution and thickness of graphene oxide platelets were assessed by AFM scans and analysed by a picture preparing program, Image J (Image Pro-Express, Version 5.0.1.26, Media Cybernetics Inc.) and Gywddion for the surface area calculation. The concentration of treated graphene oxide solution was identified by the standard curve derived from the absorption of standard solutions at the maximum peak at 230 nm. The data of mechanical properties of the materials were collected and processed via OriginLab with mean value, standard deviation and uncertainties calculated.

Chapter 4: Differentiation of graphene oxide platelets

In this chapter, the differentiation of graphene oxide platelets is discussed in detail. Section 4.1 introduces how different sized graphene oxide platelets are processed, and their characterisations and analysis. Section 4.2 illustrates how GO platelets with a different concentration are achieved using UV-Vis spectroscopy.

4.1 Size Differentiation

There are multiple factors affecting the size of GO platelets. The parameters to be discussed in this project includes the time of sonication, the centrifugation effect, and the sonication temperature.

Fig 4.1 shows the AFM images of GO platelets subject to different treatments. It is found that after sonication for 1-hour, pristine GO platelets (Fig 4.1 (a)) are split into platelets with much smaller size (Fig 4.1 (b)), and further centrifugation process allows a selection of platelets with a much more even size distribution (Fig 4.1 (c)). It is worth noting that the number of GO platelets in AFM images are not considered as a factor for analysis as the concentration of GO platelets could differ through the drop-casting process.

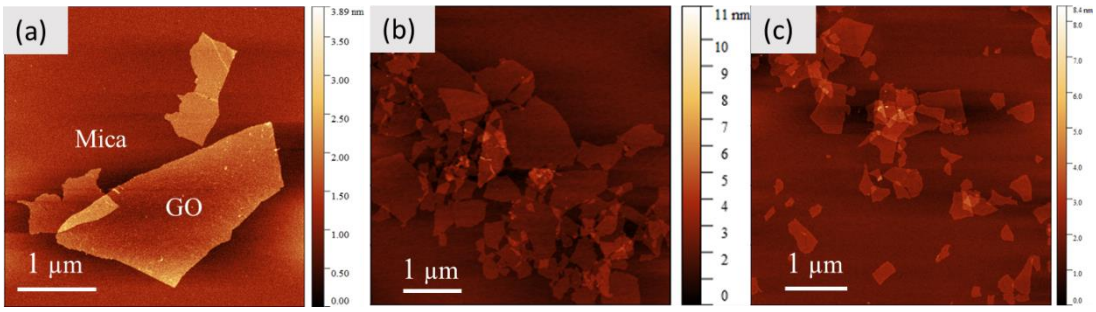

Figure 4. 1 AFM images of (a) pristine GO, (b) GO subject to 1-hour ultrasonication, (c) GO subject to 1-hour sonication and centrifugation

For quantitative analysis, a topography was acquired on GO platelets on a mica substrate. Fig 4.2 shows the AFM topography image that measured GO platelets deposited on a mica substrate. The thickness of the GO platelet is 0.8 nm from the height profile from the topography image, which is consistent with the literature[75, 76]. Due to the presence of covalent bonding with oxygen, it is known that GO is significantly thicker than pristine graphene (~0.34 nm).

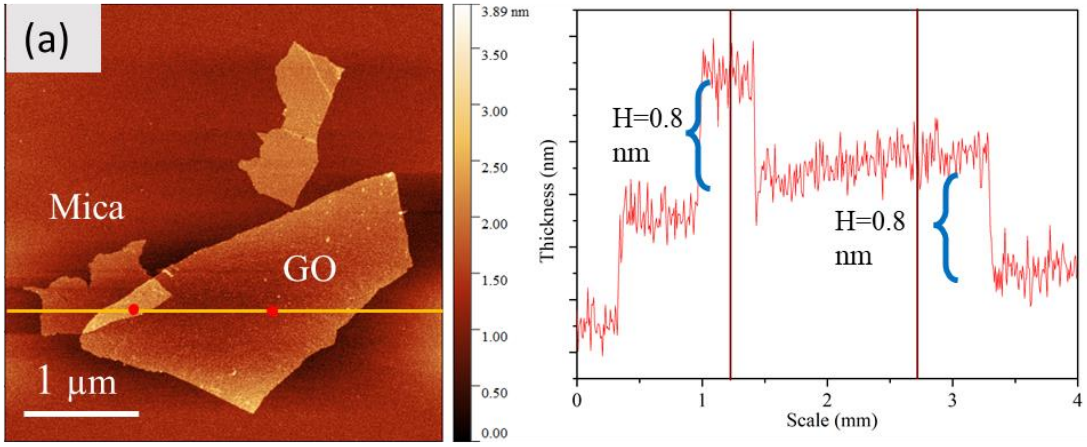

Figure 4. 2 AFM images and topography of (a) pristine GO on a mica substrate

4.1.1 Time of Ultrasonication

Time of ultrasonication also plays a role in size differentiation. It is observed that when there is an increase in sonication time, smaller GO platelets could be obtained after being centrifugated at the same speed and time. The size of GO platelets subject to1 hour and 2 hours sonication is observed more diverse (Fig 4.3 (a), (b)), compared to 3-hour and 4-hour sonication. After being sonicated for 5 hours, the average particle size increased because GO platelets started to aggregate and formed clusters, which could be also seen in those images subject to 5 and 6 hours, circled in Fig 4.3 (c) and (d). The analysis of average size was carried out using a diluted sonicated solution of GO-3hr and GO-4hr. In the case of supernatant

solution GO- 3hr (Fig 4.4 (a)), the average platelet size was 7326 nm^2 in surface area and was 47.2 times higher than GO- 4hr supernatant solution (Fig 4.4 (b)). The obtained results indicated the destructive effect of ultrasonication on GO platelets and the decrease of the average GO platelets was caused by defragmentation.

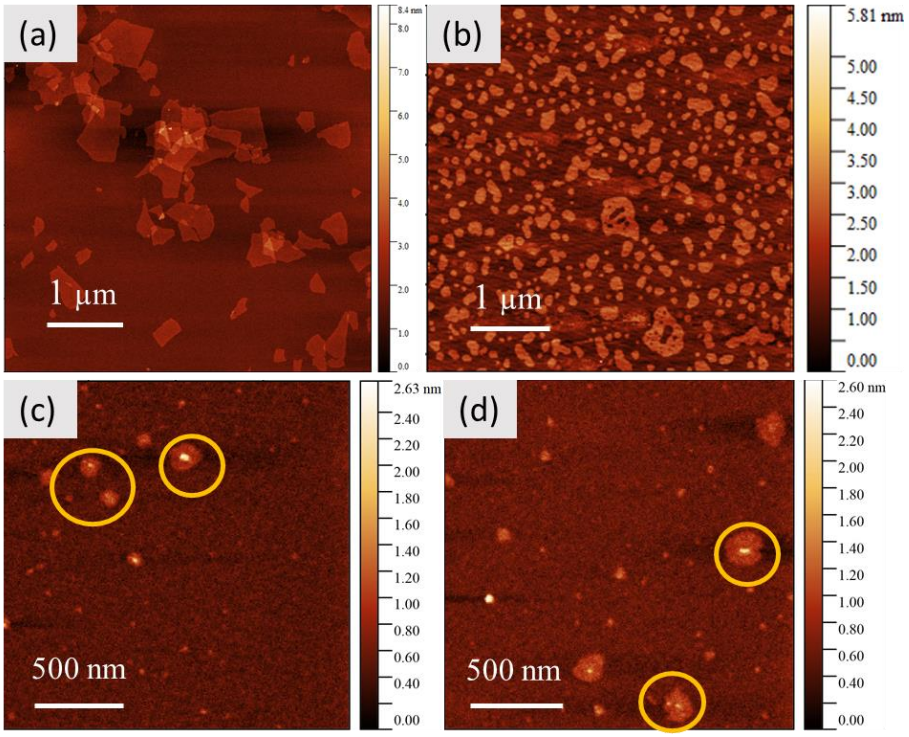

Figure 4. 3 AFM images and topography of (a) GO-1hr, (b) GO-2hr, (c) GO-5hr and (d) GO-6hr on a mica substrate

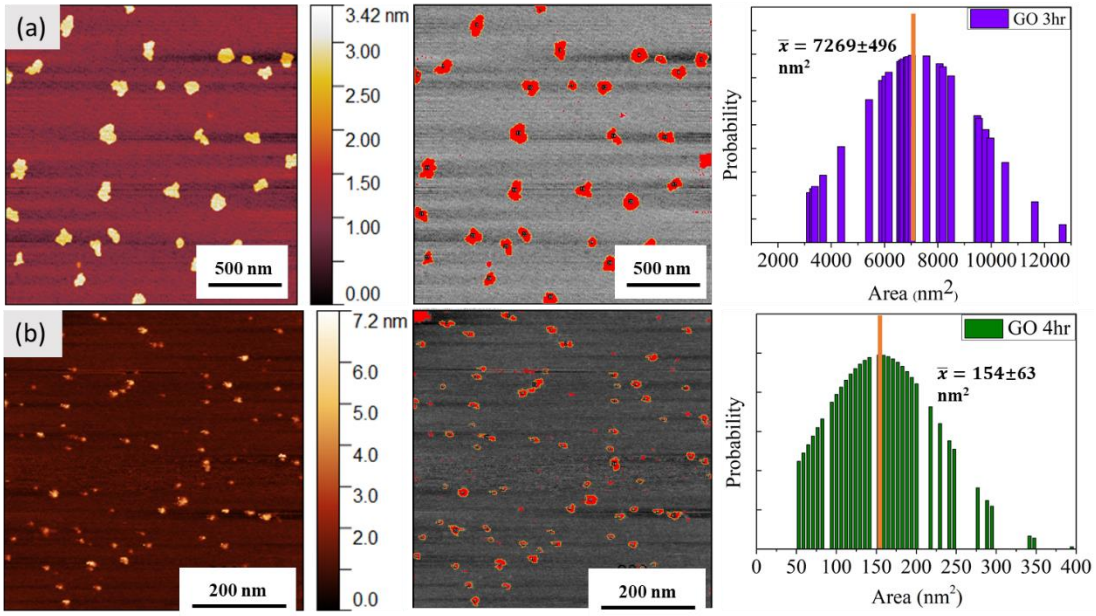

Figure 4. 4 AFM images, Gwydion image analysis and platelet size distributions (in nm^2) of (a) GO-3hr, (b) GO-4hr

4.1.2 Temperature of Ultrasonication

Additionally, the temperature of ultrasonication has an impact on the GO platelets. In this project, the study of temperature effect is mainly used to ensure the supernatant solutions are sufficiently concentrated to be added to PVP polymer later in the experiment without further drying treatment. Therefore, GO platelets subject to ultrasonication at a different temperature were not thoroughly analysed in terms of their structure, thickness, and size. Fig 4.5 shows the difference in concentration of GO supernatant solutions using a different temperature of sonication bath. It can be observed that sonication carried on in ice-bath resulted in a more concentrated supernatant solution in most studied sonication time, indicated by a darker colour in comparison to those sonicated at RT. In this project, GO platelets added in PVP polymer were those subject to sonication in ice-bath. The study of GO platelet size

using AFM has been discussed above in detail, whereas their concentration study is covered in Section 4.2.

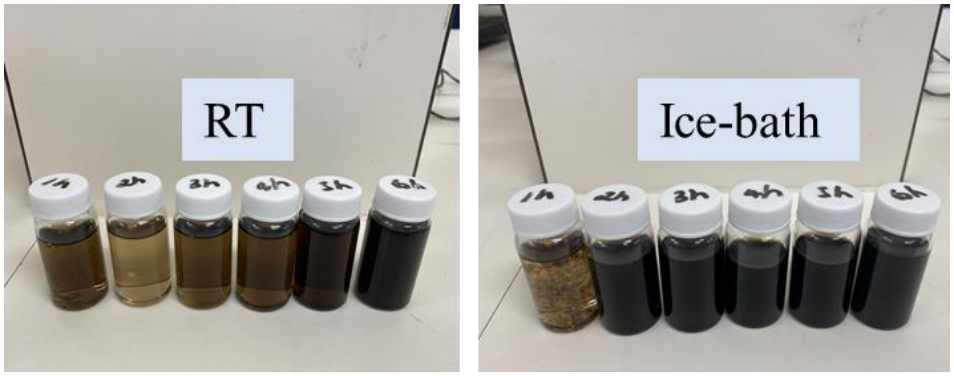

Figure 4. 5 Sample vials containing GO -1 hr, GO-2hr, GO-3hr, GO-4hr, GO-5hr and GO-6hr subject to ultrasonication at room temperature (Image on the left) and at ice bath (0-4°) (Image on the right)

To assess whether the sonication process affect the functional groups attached to graphitic carbon plane, FT-IR spectra of GO-3hr and GO-4hr has been studied. The FT-IR spectra of GO revealed that pristine GO has a lot of functional groups present in the structure (Fig 4.6). The most notable broad peak can be observed at 3400 cm^{-1}, which can be assigned mainly to residue water and hydroxyl groups[77]. A very intensive peak around 1080 cm^{-1} can be also attributed to hydroxyl groups. The peak around 1600 cm^{-1} is assigned to C=C bonds present in graphitic carbon. Peaks observed at around 1720 cm^{-1} show the presence of C=O bonds, mainly carboxyl groups, and epoxy (C-O-C) groups are present with the visible peak around 1200 cm^{-1}[178]. The treated GO platelets shared mostly the same functional groups as shown except a less pronounced peak assigned to water and hydroxyl groups at 3400 cm^{-1}. This could be due to the fact that GO platelets with a smaller surface size were more thoroughly and efficiently dried at the same drying conditions.

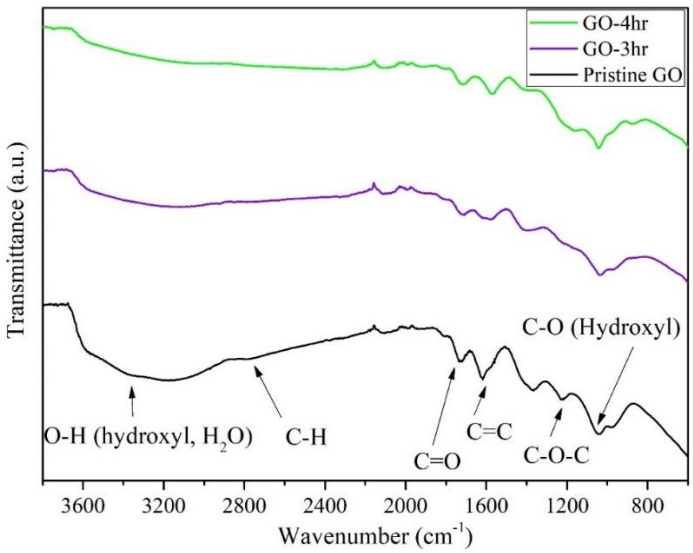

Figure 4. 6 FT-IR spectra and peak assignment of Pristine GO, GO-3hr, and GO-4hr

4.2 Concentration

The standard GO solutions exhibit ultraviolet-visible absorption spectra at the maximum absorption peak at 232 nm, which is attributed to a π-π* transition of C=C bonds (Fig 4.7 (a)). Treated GO supernatant solutions were stable with no indication of coagulation even after several months except GO-1hr shown in Fig 4.5. In this project, the concentration of GO-3hr and GO-4hr were studied in detail due to their proper platelet size. According to the Lamber-Beer law, as mentioned in Section 3.1.1, the absorbance of a sample is proportional to the concentration when the light path is the same at a given wavelength. Existing literatures stated the shift of maximum peak dependent on multiple factors including lateral size, the number of layers and surface functional groups. In the previous section, the number of layers, known as the thickness of GO platelets, were analysed by AFM and both GO-3hr and GO-4hr were around 0.8 nm. The surface functional groups were analysed by FT-IR spectra, indicating a reduction of hydroxyl group in GO platelets dried from GO-3hr and GO-4hr mostly due to the reduction of residue water. In other words, the most

pronounced variant to be considered here is the lateral size of GO-3hr and GO-4hr in comparison to the pristine GO. In established study, it is expected that GO dispersion with smaller platelets gives a smaller absorption coefficient[79]. However, there was minimal peak shift observed in Fig 4.7 (b), both remained around 230 nm (229.6 for GO-4hr and 230.1 for GO-4hr). The absorbance of GO-3hr and GO-4hr was taken at 230 nm wavelength for the simplicity when plotted to the standard curve of absorbance versus concentration $A = 48.4554c + 0.0434$ (Fig 4.7 (c)). The concentration of GO-3hr and GO-4hr were calculated as 0.0437 mg/mL and 0.0482 mg/mL.

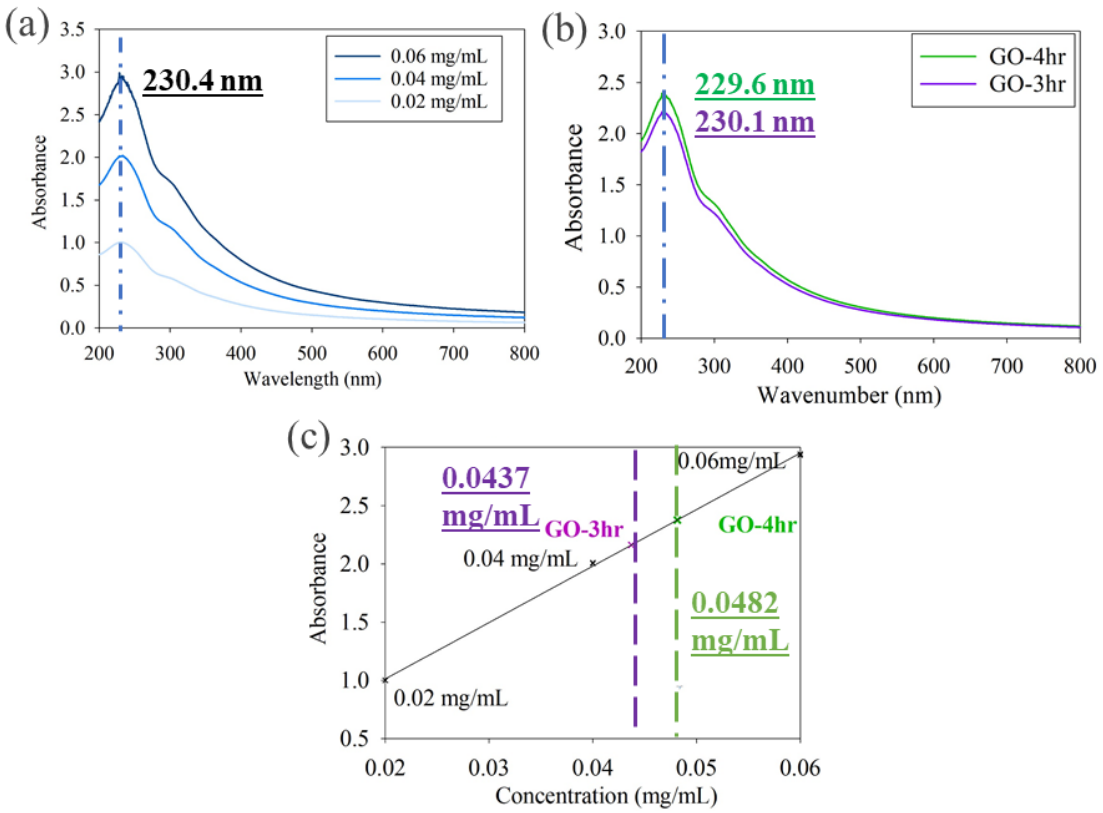

Figure 4. 7 UV-Vis absorption spectra of (a) three standard GO solutions with different concentrations, showing a maximum peak at 230.4 nm and (b) GO-3hr and GO-4hr; (c) The plot of a standard curve divided by absorbance (λ=230 nm) as a

function of concentration for three standard GO solutions. The concentration of GO-3hr and GO-4hr is determined using the slope of the curve.

Chapter 5: Electrospinning of PVP polymer and PVP composite

In this chapter, the characterisation of electrospun PVP nanofiber and PVP-GO composite nanofibers is discussed in detail. Section 5.1 discusses the change in diameter size under different electrospinning parameters. Section 5.2 illustrates how the addition of GO platelets affect PVP nanofiber diameter by varying their platelet size and concentration.

5.1 Electrospinning of Pure PVP

Nanofibers with a diameter ranging from 100 to 300 nm are required in this project. A concentration of 20 wt.% PVP solution has been used in this project to reduce bead formation[48]. To obtain nanofibers in this desired range, electrospinning parameters were optimised using different collection distances (8 cm to 10 cm), a range of voltage (7-10 kV), and feed rate (0.2-0.4 mL/hr). The effect of electrospinning parameters on mean fibre diameter of PVP polymer is presented in Table A.1 Appendix A.

5.1.1 Effect of Collection Distance

The electrospinning of PVP solution in DI water at a collection distance between 8 to 10 cm was performed. The mean fibre diameter reduced with an increase in tip to collector distance. This could be explained that the increased collector distance, total path trajectory of the jet increases, allowing more stretching of the jet during its travel to the collector plate.

5.1.2 Effect of Electric Field

The electrospinning of PVP solution in DI water at a power supply between 7 to 10 kV was performed. The fibre diameter distribution of PVP polymer decreased with an increasing in electrospinning voltage from 8 kV to 9 kV. This is because an increase in the amount of charge flowing in a jet increases the repulsion force, resulting in an increased stretching force acting on the polymer jet. This leads to the development of thinner fibres. Also, it was observed that beads started to form when voltage increased to 10 kV (Fig 5.1 (a)) due to the increased electric field intensity that influenced fibre generation, while no visible fibres were collected when the voltage reduced to 7 kV.

5.1.3 Effect of Flow Rate

Feed rate is another factor that affects the morphology of the electrospun fibres. With an increased feed rate, the mean fibre diameter increased slightly. Feed rate has a lesser effect on the mean fibre diameter but is found most crucial electrospinning parameter for the bead reduction as it the bead formation is effectively suppressed when the feed rate is adjusted to make a stable Taylor cone against the applied voltage (Fig 5.1 (b)).

In a word, the distance between the needle tip and metal collector is found to one of the parameters that mostly affect the mean fibre diameter, while the voltage and feed rate have significant effects on the bead formation. SEM image and fibre diameter size distribution of PVP at optimum electrospinning parameters (9 kV power supply, 8 cm collection distance and 0.3 mL/hr feed rate) with no visible beads formed shown in Fig 5.1 (c,d), with a mean fibre diameter of 315 nm. The

mean diameter of electrospun nanofiber using other parameters were included in Table A.1 in Appendix A.

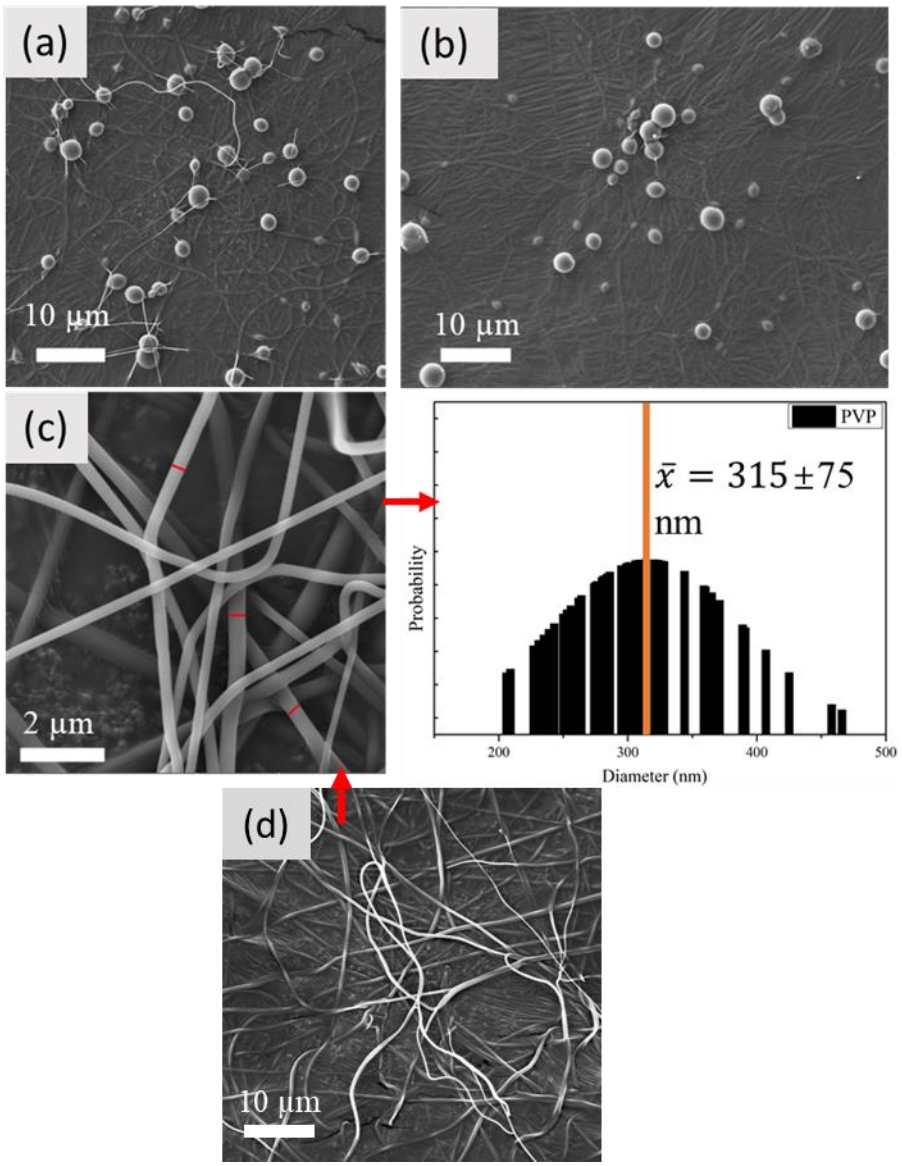

Figure 5. 1 SEM images of (a) PVP nanofiber with parameters of 10 kV power supply, 8 cm collection distance and 0.3 mL/hr feed rate, (b) PVP nanofiber with parameters of 10 kV power supply, 8 cm collection distance and 0.2 mL/hr feed rate, (c) PVP nanofiber with optimal parameters of 9 kV power supply, 8 cm collection distance and 0.3 mL/hr feed rate, and their diameter distribution, (d) Zoomed-out SEM image of PVP nanofiber of (c)

5.2 Electrospinning of PVP-GO Composite

The electrospinning of PVP composite used the same optimal electrospinning parameters for PVP polymer. SEM images and fibre diameter size distribution are shown in Fig 5.2 and Table 5.1. It is worth noting that the mean diameter decreased when a higher concentration of GO platelets was added and had a smaller variation in diameter distribution, indicated by a smaller standard deviation (Fig 5.2 (b) and (d)). This may be attributed to the fact that a higher concentration of GO in polymer solution increases the conductivity of the polymer solution, which promotes the force to escape the columbic repulsion force, and hence, it results in thinner and even fibres collected on the target plate. The size of GO platelets did not play a significant role in changing mean fibre diameter when the concentration of GO platelets was 0.1 wt. %, whereas smaller GO platelets (GO-4hr) seemed to result in a larger electrospun nanofibers when the GO concentration was at 0.2 wt.%.

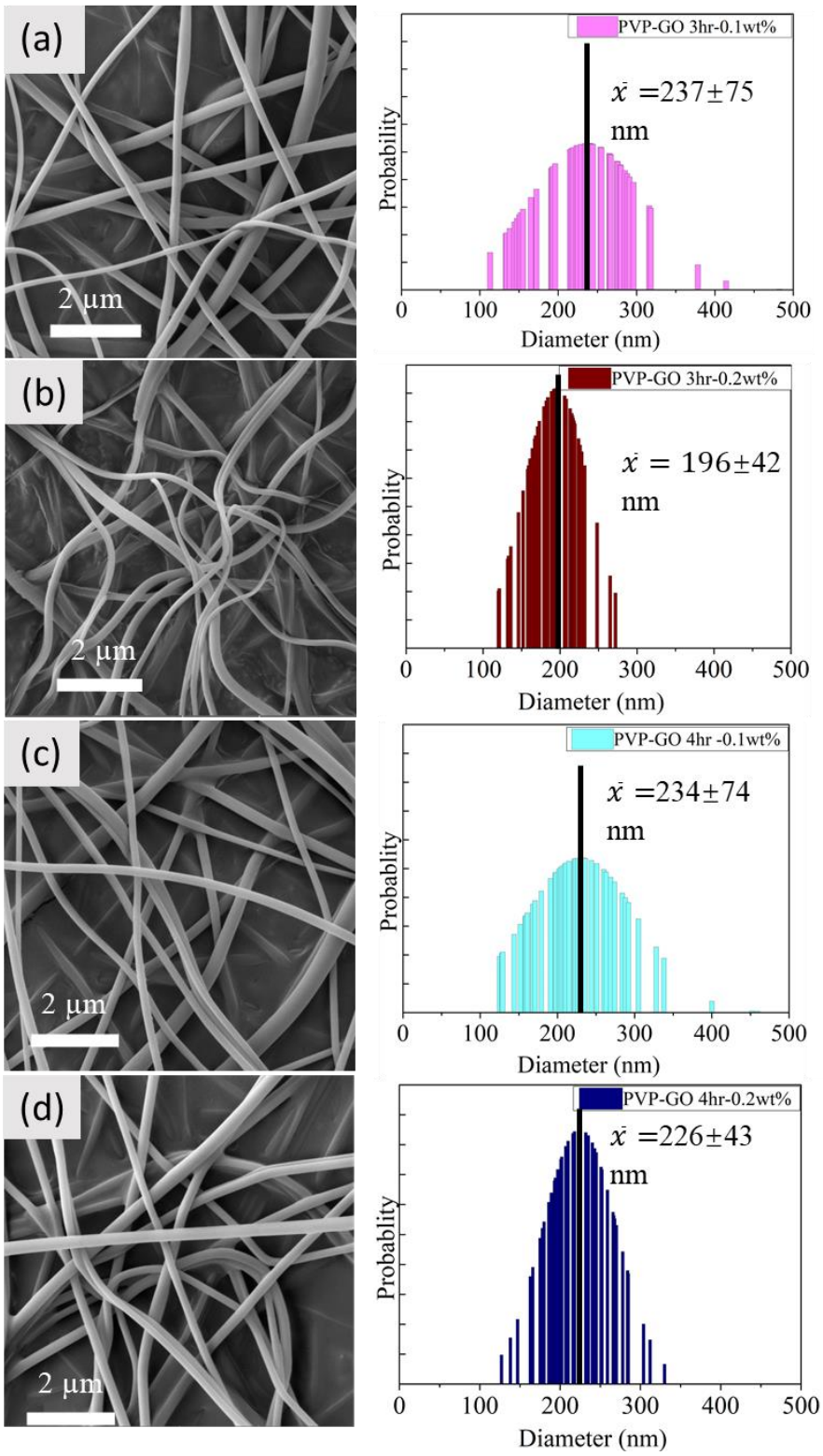

Figure 5. 2 SEM images and diameter distribution of electrospun (a) PVP-GO-3hr-0.1wt%, (b) PVP-GO-3hr-0.2wt%, (c) PVP-GO-4hr-0.1wt%, and (d) PVP-GO-4hr-0.2wt%

Table 5. 1 Summary of diameter of electrospun PVP-GO nanofibers

Nanofiber	Diameter (nm)
PVP-GO-3hr-0.1wt%	237±75
PVP-GO-3hr-0.2wt%	196±42
PVP-GO-4hr-0.1wt%	234±74
PVP-GO-4hr-0.2wt%	226±43

Raman analysis confirms the existence of GO embedded in PVP polymer shown in Fig 5.3. There are several characteristic components for pure PVP, which are attributed to C-C ring and chain, CH_2 twist, C-N stretch and amide[77]. The G band (at ν=1348 cm^{-1}) corresponds to a E2g in-plane vibration of the C-C bonds and the D band (at ν=1600 cm^{-1}) is associated with disorders, dopants or functionalised atoms and edges in the graphene layers that decrease the sp^2 carbon domain and the C-C bond stretch with sp^2 carbon formation (G band), which is commonly seen in GO[77]. The degree of defect loading the disorder in the structure can be determined by the intensity ratio of the D band to G band (I_D/I_G). The I_D/I_G ratio of different PVP-GO nanofibers is calculated as shown in Table 5.1, indicating that the GO platelets have large domains of oxygen containing functional groups mixed with sp^2 carbon in graphitic planes.

	I_D	I_G	I_D/I_G
PVP-GO-3hr-0.1wt%	626.25	606.23	1.03
PVP-GO-3hr-0.2wt%	2547.76	2454.76	1.03
PVP-GO-4hr-0.1wt%	1864.16	1809.19	1.03
PVP-GO-4hr-0.2wt%	6002.71	5775.22	1.04

Table 5. 2 Summary of I_D/I_G of PVP-GO nanofibers

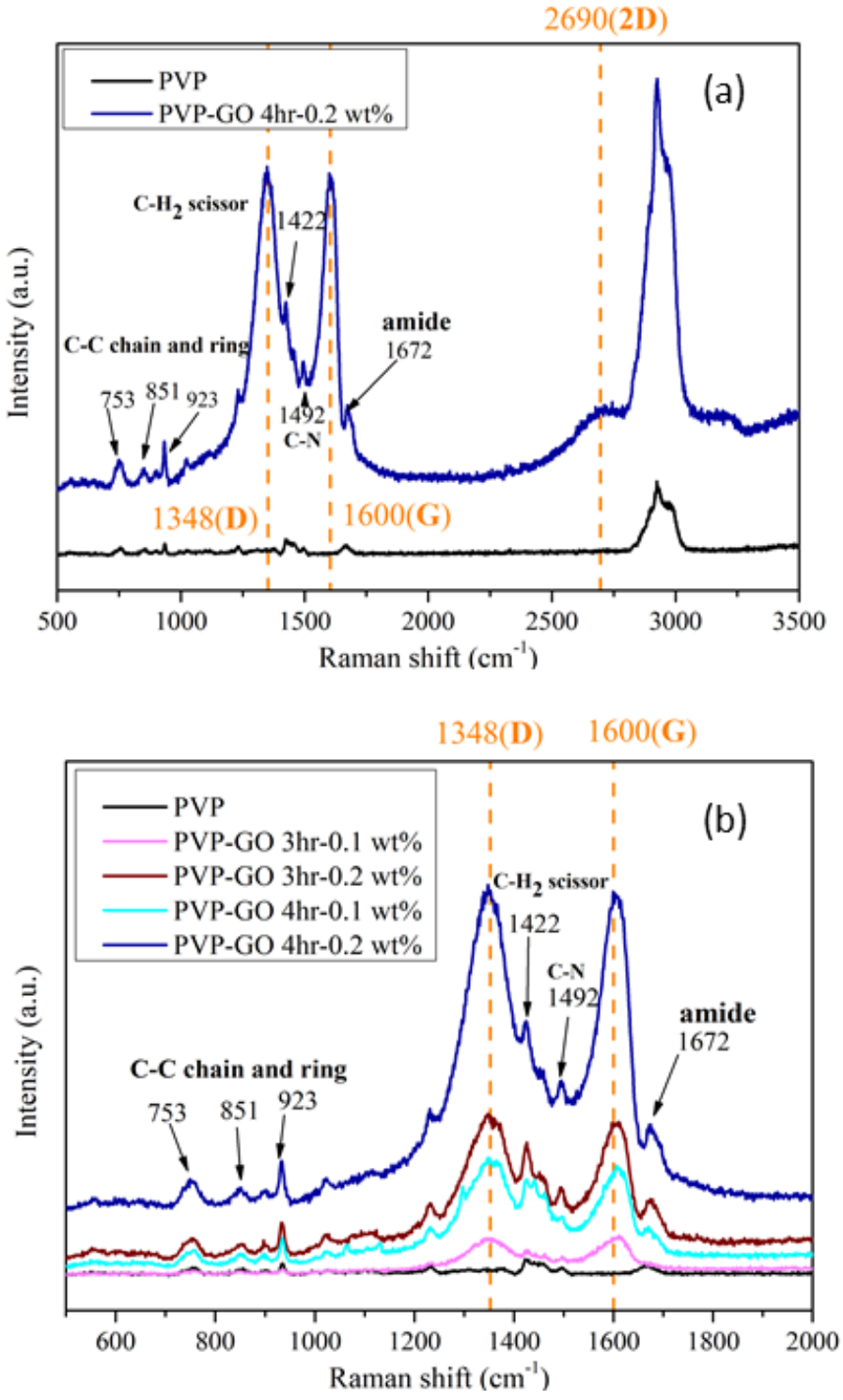

Figure 5. 3 Raman spectra of (a) PVP and PVP-GO-4hr-0.2wt% with wavenumber ranging from 500-3500 cm^{-1} and (b) PVP, PVP-GO nanofiber composites with wavenumber ranging from 500 to 2000 cm^{-1}

Chapter 6: Mechanical properties of polymeric material

In this chapter, the mechanical properties of PVP nanofiber and PVP-GO composite nanofibers is discussed in detail. Section 6.1 discussed the mechanical properties of bulk polymeric material including pure PVP and PVP-GO composites. Section 6.2 discussed the mechanical behaviours of electrospun PVP and PVP-GO nanofibers using nanoindentation techniques.

6.1 Mechanical Properties of Bulk Polymeric Material

Considering the high strength of GO platelets, it was expected that the addition of GO platelets into polymer could potentially improve the mechanical properties of the bulk composite.

The force-displacement curves shown in Fig 6.1 consist of loading, holding, and unloading of the Berkowitz indenter tip into PVP and PVP-GO composite bulk materials. The loading curves show a tip indenting into a material with an increase in displacement, also known as indentation depth, when applying increasing force to the bulk material. The holding curves shows that the displacement keeps constant with a decrease of force. The unloading curves show the tip moving away from the measured material with a decreased force. The reduced elastic modulus of the bulk materials was derived from the slope of the unloading curve at its maximum force.

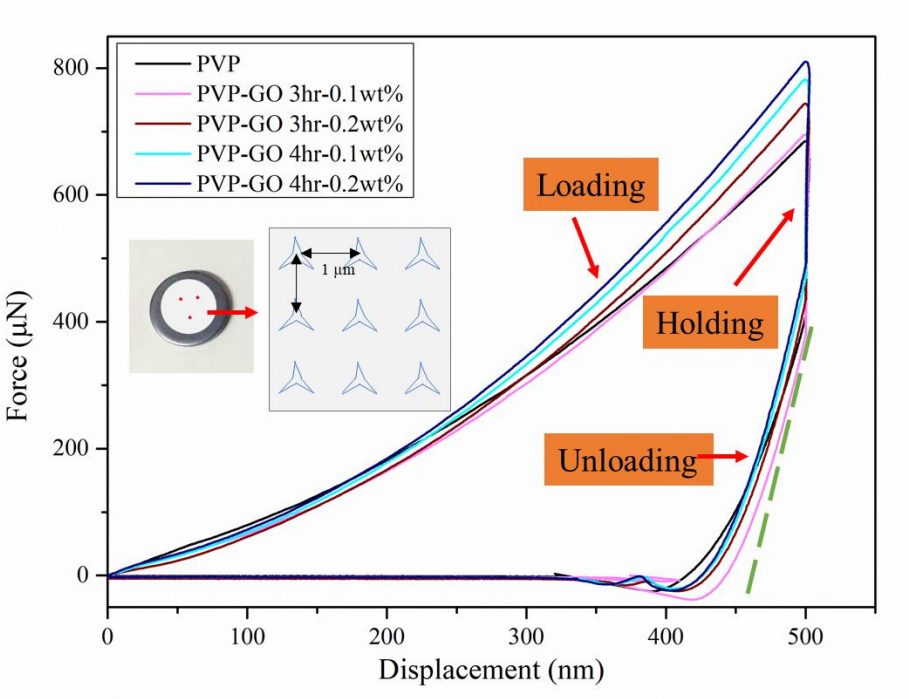

Figure 6. 1 Representative Force-displacement (F-h) curves of PVP and PVP-GO bulk materials

Exiting literature reported E of bulk PVP polymer ranging from 1.6 GPa to 3.5 GPa depending on the molecular weight of the polymer[80]. The average Young's Modulus of pure bulk PVP was calculated as 2.837 GPa, which is within this reference range (Fig 6.2). All bulk materials were measured on a randomly picked region three times and each region consisted of a 3 × 3 matrix with each test point 1 μm apart from each other (Fig 6.1). The addition of GO platelets increased Young's Modulus and Hardness of the bulk material added with a higher concentration and smaller sized GO platelets (PVP-GO-4hr-0.2 wt.%), which exhibited a highest Young's Modulus and Hardness (Fig 6.2).

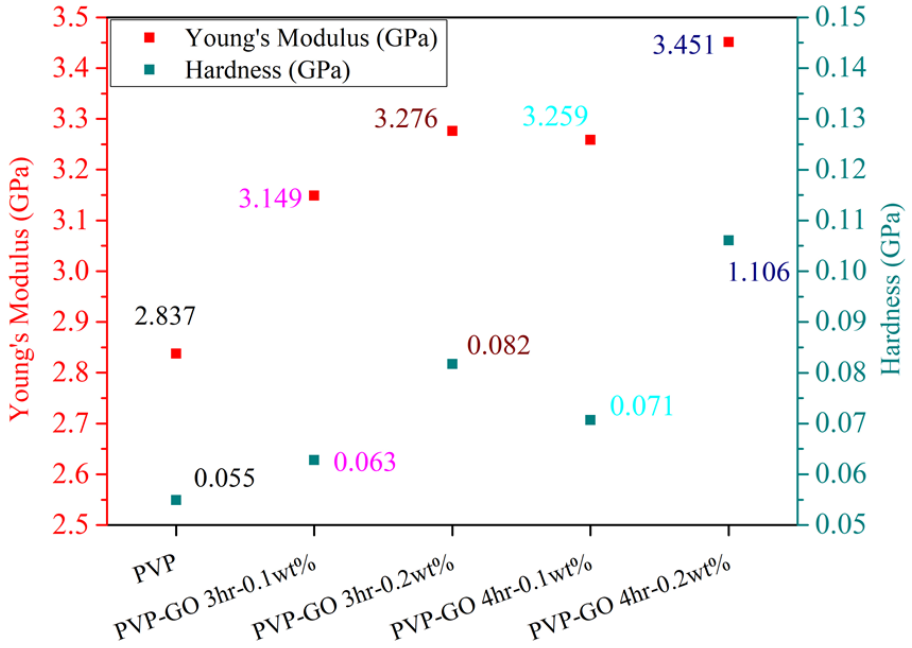

Figure 6. 2 Young's Modulus (E) and Hardness of PVP and PVP-GO bulk material

GO platelets acted as reinforcement of the polymer matrices with a high surface area-to-volume ratio. Once GO introduced into the polymer matrix, it is expected that they interact with PVP chain at the molecular level, and the strong interfacial interactions enable efficient stress transfer from a mechanically weaker polymer matrix to a mechanically superior nanocarbon particles. Apart from increasing the mechanical elasticity, indicated by an increased Young's Modulus, the interactions also increased the plastic flow resistance of the polymer matrix, in turn leading to an increased hardness. Due to sp^2 hybridisation and a larger number of reactive lattice defects on the surface of GO, bulk polymer samples added with smaller sized and higher concentration GO platelets tend to form more strong bonds with polymer chains due to more active bonding sites compared to polymer samples added with larger sized and lower concentration GO platelets. As has been reported by other studies, when smaller particles are applied as a filler in polymeric composite material, the thermal contraction process is present in the starting points of the measurement, mostly homogeneously. This gives a nearly homogeneous and higher

modulus material[81]. This may at least in part explain highest Young's Modulus of PVP-GO 4hr-0.2wt% observed among all samples.

6.2 Mechanical properties of PVP and PVP-GO Nanofiber

It was challenging to measure mechanical properties of nanofibers using nanoidentation techniques due to multiple factors including the hole size and self-adhesion between nanofiber and substrate. In this project, three bending point tests were attempted to study elastic properties of PVP and PVP-GO nanofibers, however needing further investigations. Instead, the initial contact stiffness of nanofibers was measured.

6.2.1 Three Point Flexural Tests

To investigate the mechanical behaviour in the elastic range of the material until failure, three-point bending tests were carried out. However, there are multiple challenges when performing three point bending tests for samples in a nanoscale using nanoindentation techniques. A conical tip was used in the three-point bending tests to ensure a sufficient contact area while not too sharp to cut the nanofiber.

In this project, nanofibers were electrospun on a substrate with pre-cut holes (depth of 1 µm) at a controlled setting to ensure minimal formation of fibre networks on the tested site. There were three different sized hole pre-cut including 40 µm, 20 µm and 10 µm in diameter. Fig 6.3 illustrates the PVP nanofibers electrospun on a glass substrate with different hole sizes. It is clearly observed that hole size of 20 µm (Fig 6.3 (c)) enables a better electrospinning result to get a single fibre sitting on top in comparison to hole size 10 µm (Fig 6.3 (d)). Hole size of 40 µm is considered

too big since the fibre either experienced collapse or incomplete bending after the nanoindentation tests (Fig 6.3 (a) and (b)).

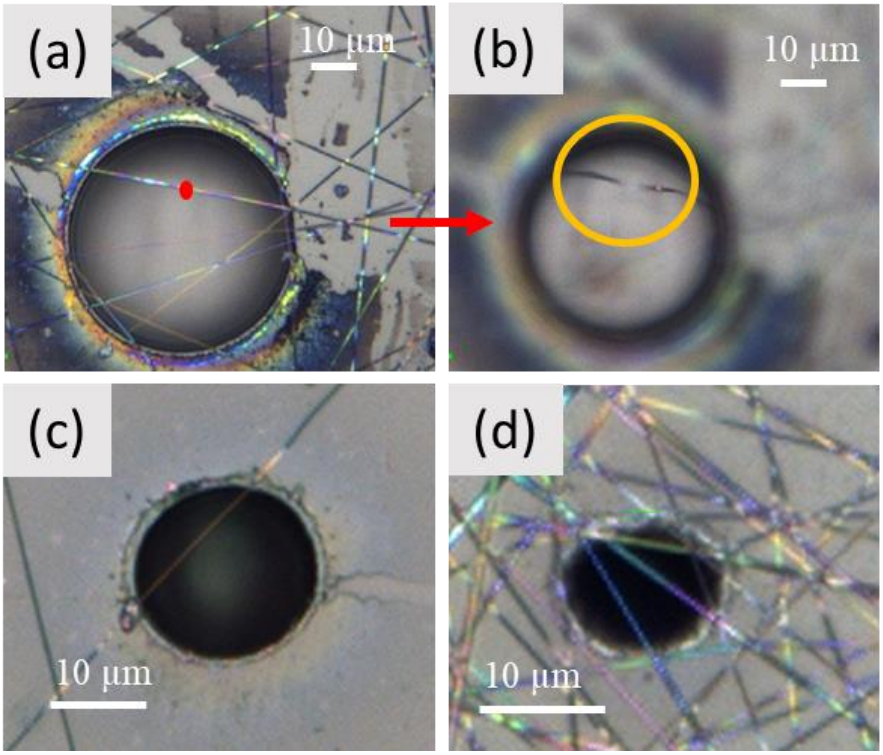

Figure 6. 3 Microscopic images of (a) Pre- (b) Post-indentation tests of PVP nanofiber electrospun on a 40 µm diameter hole, (c) a single PVP nanofiber electrospun on a 20 µm diameter hole, (d) PVP nanofibers electrospun on a 10 µm diameter hole

The second challenge observed is the insufficent self-adhesion between a nanofiber and a plain glass slide as substrate shown in Fig 6.4, indicated by a slight movement of two ends of nanofiber after the indentation test.

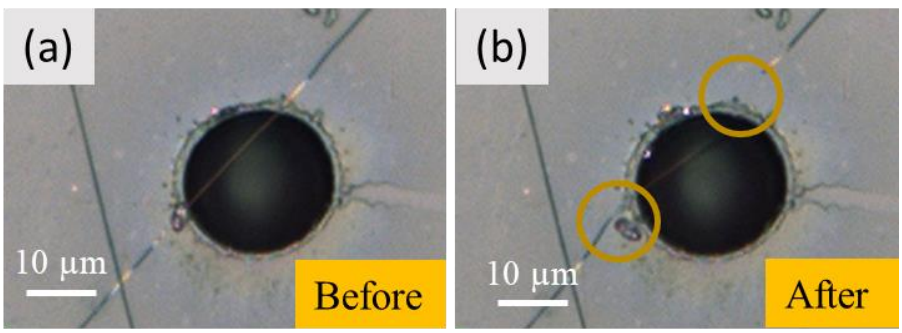

Figure 6. 4 Microscopic images of (a) Pre- and (b) Post-indentation tests of a PVP nanofiber electrospun on a 20 µm diameter hole

This gave rise to the use of electron-beam induced deposition process using platinum plasma via a FIB-SEM (Focused Ion Beam- SEM). However, it was observed that the platinum plasmas deformed the PVP nanofiber with bulged end close to the platinum deposition site and fibre surface appeared rougher than the rest (Fig 6.5). This introduced the variants of sample deformity and thus nanoindentation tests were not performed on platinum fixed nanofibers.

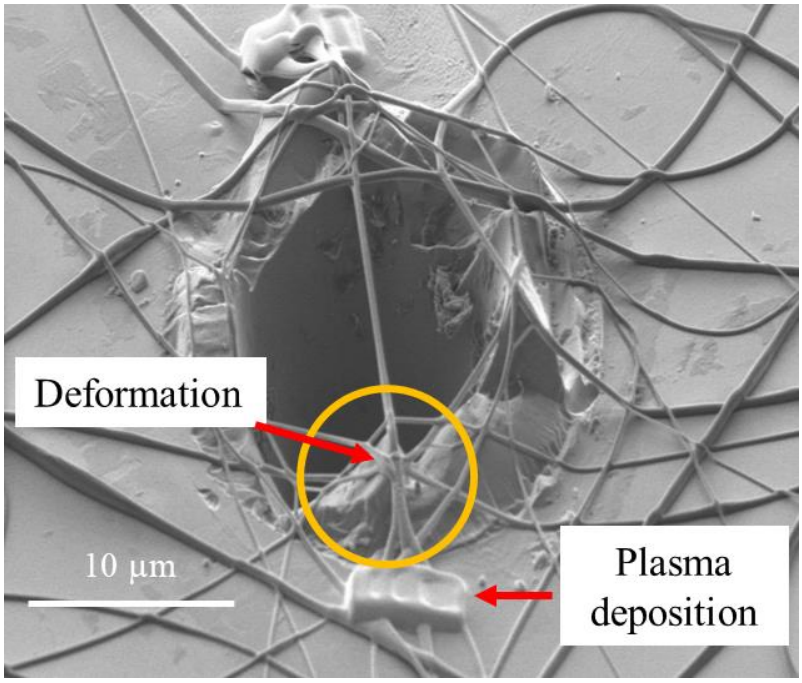

Figure 6. 5 SEM image of PVP nanofibers electrospun on a silicon wafer with two ends fixed using platinum plasma

Then, further investigations on different substrates were performed to obtain a substrate with an enhanced self-adhesion of nanofiber and substrate than plain glass. Among different factors, surface roughness of substrate was investigated via AFM. Three substrates were studied in this project including the plain glass, glass coated with 10 nm gold and FTO glass. It was observed previously that plain glass was too

smooth to hold PVP nanofibers, which makes FTO glass the best substrate among the studied substrates with Ra 8.36 nm (Fig 6.6 (c)). However, it was still observed that the nanofiber slightly moved even with FTO glass, which left me the option to study the mechanical behaviour using a conventional indentation test on a substrate.

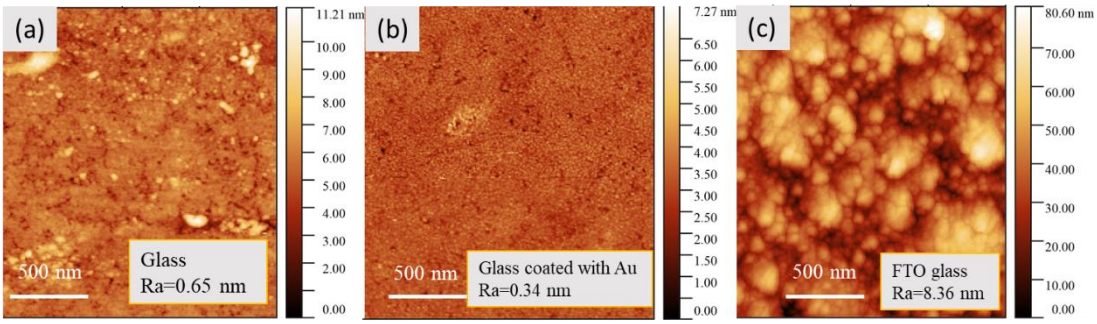

Figure 6. 6 AFM images of (a) Glass, (b) Glass coated with Au, (c) FTO glass

6.2.2 Initial Contact Stiffness

In the indentation test of nanofibers, the displacement was set to 80 nm for the tip to indent into the material. FTO glass was used as the substrate and a Berkovich diamond tip was used to indent into the nanofiber. However, due to the size of nanofiber ranging from (196 nm to 315 nm), force-displacement curves were observed to be easily affected by the substrate after the tip indented more than 10 nm into the material. It is not appropriate to use conventional contact stiffness to assess the mechanical properties of nanofibers which is usually calculated by the slope of the fit for upper portion of the unloading curve (Fig 6.1). Instead, the initial contact stiffness defined as the slope of the fit for lower portion of the loading curve was assessed because it had minimal substrate effect. It is found that the addition of GO increased the initial contact stiffness of PVP nanofiber (Fig 6.7 and Table 6.1). With an increase in concentration of the GO platelets added, there was an increase in the

initial contact stiffness for both sizes of GO platelets. A smaller size of GO platelets enabled a higher initial contact stiffness at the same GO concentration.

Due to the substrate effect, the elastic modulus and hardness of nanofibers cannot be properly measured and compared to the bulk PVP and PVP-GO materials. However, the results of initial contact stiffness are consistent with what has been discussed for bulk PVP and PVP-GO composite above (Section 6.1) that a higher concentration and a smaller platelet size improved the mechanical behaviour of the material. Additionally, it is also worth noting that the concentration plays a more significant role in increasing the initial contact stiffness from 214 N/m to 3654 N/m for PVP-GO-3hr-0.2w% and to 4689 N/m for PVP-GO-4hr-0.2wt% nanofibers.

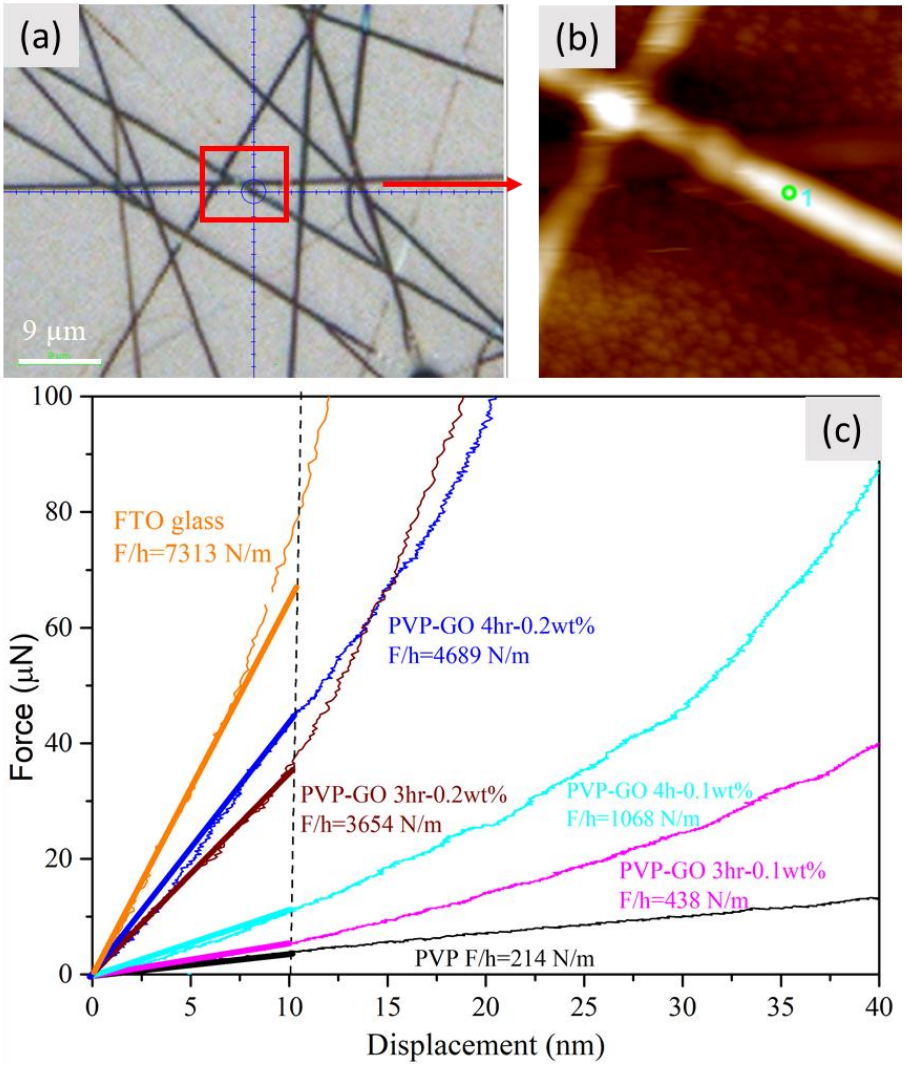

Figure 6. 7 (a) Microscopic image of PVP nanofibers, (b) AFM scan of boxed area of nanofibers, (c) Representative force and displacement (F-h) curves of PVP and PVP-GO nanofibers with initial contact stiffness calculated

Table 6 1 Summary of initial contact stiffness of nanofibers and substrate

Nanofiber/substrate	**Initial contact stiffness (Fh^{-1})**
PVP	214
PVP-GO-3hr-0.1%	438
PVP-GO-4hr-0.1%	1068
PVP-GO-3hr-0.2%	3654
PVP-GO-4hr-0.2%	4789
FTO glass	7313

Chapter 7: Conclusions

7.1 Conclusions

This project studied the effects of GO on the mechanical behaviour of the PVP composite material in form of bulk and nanofiber by varying (1) size of GO platelets, (2) concentration (in weight percentage). The choice of the material was based on the literature review of the existing research. Moreover, novel approaches were selected to study the aims and topics of this project, which were extensively discussed in Chapter 4 to 6 in the thesis. The properties of treated GO platelets were studied from both qualitative and quantitative aspects. The mechanical properties of bulk material and nanofibers were studied in detail by nanoindentation techniques. The following conclusions have been drawn.

In Chapter 4, the factors that affect the size differentiation of GO platelets have been discussed and it can be concluded that (1) an increased time of ultrasonicate results in a smaller platelet size while an extensive sonication time could lead to the aggregation of platelets. (2) The centrifugation process allows the selection of GO platelets with an evener size distribution. (3) A lower temperature of ultrasonication resulted in a more concentrate supernatants of centrifugated GO suspension.

In Chapter 5, the effects of electrospinning parameters on PVP and PVP-GO nanofibers have been discussed and can be concluded that at a given concentration of polymer solution (20 wt.% in DI water) (1) the distance between the needle tip and metal collector is found to one of the parameters that mostly affect the mean fibre diameter. (2) The voltage and feed rate have significant effects on the bead formation. (3) Desired fibre diameter of PVP and PVP-GO can be obtained at

optimum electrospinning parameters (9 kV power supply, 8 cm collection distance and 0.3 mL/hr feed rate). (4) The mean fibre diameter decreased with a higher concentration of GO platelets added and had a smaller variation in diameter distribution. (5) Smaller GO platelets resulted in a larger electrospun nanofibers at the GO concentration of 0.2 wt.%

In Chapter 6, the mechanical properties of bulk material and electrospun PVP and PVP-GO nanofibers have been investigated. It can be concluded that (1) the bulk material added with a higher concentration and smaller sized GO platelets (PVP-GO-4hr-0.2 wt.%) exhibited a highest Young's Modulus and Hardness. (2) The concentration of GO plays a more significant role in increasing the initial contact stiffness of nanofibers.

7.2 Limitations and Future work

This work implements qualitative and quantitative analysis of graphene oxide platelets and polymeric materials. There are several limitations to this research and many aspects need to be improved.

- The percentage of GO added to polymeric solution prior to electrospinning was calculated by the maximum peak at wavelength 230 nm using UV-Vis spectra. There were minimal peak shifts of different sized graphene oxide platelets observed but for the simplicity of calculation, peak shifts were not fully investigated, and this could be further studied.
- The investigation of functional groups before and after ultrasonication treatments only included a qualitative study which could be further studied regard to their percentage and structure.

- The amount and distribution of GO platelets in polymeric bulk sample and electrospun nanofibers were not assessed. In the future, the distribution of graphene oxide platelets in polymeric nanofibers can be studied using Small-angle X-ray scattering (SAXS).
- The three point bending tests were not successful due to multiple challenges discussed in Section 6.2.1 which need to be addressed in the future
- Biocompatible tests could be conducted to assess the biocompatibility of the composite materials

7.3 Final remarks

In summary, in this work, different sized GO platelets have been prepared using ultrasonication and centrifugation techniques. The desired nanofibers have been successfully fabricated after optimising electrospinning parameters. The addition of GO in both PVP bulk and nanofibers has shown an improvement in mechanical behaviours, indicated by an increased Young's modulus, an increased Hardness and an increased initial contact stiffness. This works will provide critical information to produce new super-elastic materials, with potential applications in medicine, for the development of artificial tendons and ligaments.

Bibliography

1. Rahman, R.; Zhafer Firdaus Syed Putra, S., 5 - Tensile properties of natural and synthetic fiber-reinforced polymer composites. In *Mechanical and Physical Testing of Biocomposites, Fibre-Reinforced Composites and Hybrid Composites*, Jawaid, M.; Thariq, M.; Saba, N., Eds. Woodhead Publishing: 2019; pp 81-102.
2. Termonia, Y., Molecular modeling of particle reinforcement in elastomers: Effect of particle radius and volume fraction. *Polymer* **2010,** *51* (19), 4448-4451.
3. Xu, D. The Role of Nanofillers in Polymer Nanocomposites. ProQuest Dissertations Publishing, 2016.
4. Termonia, Y., Molecular Modeling of Spider Silk Elasticity. *Macromolecules* **1994,** *27* (25), 7378-7381.
5. Zhou, X.; Pan, Y.; Liu, R.; Luo, X.; Zeng, X.; Zhi, D.; Li, J.; Cheng, Q.; Huang, Z.; Zhang, H.; Wang, K., Biocompatibility and biodegradation properties of polycaprolactone/polydioxanone composite scaffolds prepared by blend or co-electrospinning. *Journal of bioactive and compatible polymers* **2019,** *34* (2), 115-130.
6. Chee, W. K.; Lim, H. N.; Huang, N. M.; Harrison, I., Nanocomposites of graphene/polymers: a review. *RSC Advances* **2015,** *5* (83), 68014-68051.
7. Vollrath, F.; Porter, D., Silks as ancient models for modern polymers. *Polymer* **2009,** *50* (24), 5623-5632.
8. Xing, C.; Munro, T.; White, B.; Ban, H.; Copeland, C. G.; Lewis, R. V., Thermophysical properties of the dragline silk of Nephila clavipes spider. *Polymer* **2014,** *55* (16), 4226-4231.
9. Römer, L.; Scheibel, T., The elaborate structure of spider silk: structure and function of a natural high performance fiber. *Prion* **2008,** *2* (4), 154-161.
10. Murad, A.; Rech, E., Molecular dynamics simulations of the minor ampullate spidroin modular amino acid sequence from Parawixia bistriatra : insights into silk tertiary structure and fibre formation. *Journal of Molecular Modeling* **2011,** *17* (5), 1183-1189.
11. Foong, C. P.; Higuchi-Takeuchi, M.; Malay, A. D.; Oktaviani, N. A.; Thagun, C.; Numata, K., A marine photosynthetic microbial cell factory as a platform for spider silk production. *Communications Biology* **2020,** *3* (1), 357.
12. Cao, M.; Wang, N.; Wang, L.; Zhang, Y.; Chen, Y.; Xie, Z.; Li, Z.; Pambou, E.; Li, R.; Chen, C.; Pan, F.; Xu, H.; Penny, J.; Webster, J. R. P.; Lu, J. R., Direct exfoliation of graphite into graphene in aqueous solutions of amphiphilic peptides. *Journal of Materials Chemistry B* **2015,** *4* (1), 152-161.
13. Hiremath, P.; Nuguru, K.; Agrahari, V., Chapter 8 - Material Attributes and Their Impact on Wet Granulation Process Performance. In *Handbook of Pharmaceutical Wet Granulation*, Narang, A. S.; Badawy, S. I. F., Eds. Academic Press: 2019; pp 263-315.
14. Brady, J.; Dürig, T.; Lee, P. I.; Li, J. X., Chapter 7 - Polymer Properties and Characterization. In *Developing Solid Oral Dosage Forms (Second Edition)*, Qiu, Y.; Chen, Y.; Zhang, G. G. Z.; Yu, L.; Mantri, R. V., Eds. Academic Press: Boston, 2017; pp 181-223.
15. Awasthi, R.; Manchanda, S.; Das, P.; Velu, V.; Malipeddi, H.; Pabreja, K.; Pinto, T. D. J. A.; Gupta, G.; Dua, K., 9 - Poly(vinylpyrrolidone). In *Engineering of Biomaterials for Drug Delivery Systems*, Parambath, A., Ed. Woodhead Publishing: 2018; pp 255-272.

16. Kariduraganavar, M. Y.; Kittur, A. A.; Kamble, R. R., Chapter 1 - Polymer Synthesis and Processing. In *Natural and Synthetic Biomedical Polymers*, Kumbar, S. G.; Laurencin, C. T.; Deng, M., Eds. Elsevier: Oxford, 2014; pp 1-31.
17. Li, Y.; Zhao, E.; Li, L.; Bai, L.; Zhang, W., Physicochemical and pharmacological investigations of polyvinylpyrrolidone - tetrahydroxyborate hydrogel containing the local anesthetic lidocaine. *Journal of Molecular Liquids* **2021,** *335*, 116526.
18. Franco, P.; De Marco, I., The Use of Poly(N-vinyl pyrrolidone) in the Delivery of Drugs: A Review. *Polymers* **2020,** *12* (5).
19. Li, B.; Zhang, Y.; Fu, L.; Yu, T.; Zhou, S.; Zhang, L.; Yin, L., Surface passivation engineering strategy to fully-inorganic cubic CsPbI3 perovskites for high-performance solar cells. *Nature communications* **2018,** *9* (1), 1-8.
20. Koczkur, K. M.; Mourdikoudis, S.; Polavarapu, L.; Skrabalak, S. E., Polyvinylpyrrolidone (PVP) in nanoparticle synthesis. *Dalton transactions : an international journal of inorganic chemistry* **2015,** *44* (41), 17883-1795.
21. Utkarsh; Hegab, H.; Tariq, M.; Syed, N. A.; Rizvi, G.; Pop-Iliev, R., Towards Analysis and Optimization of Electrospun PVP (Polyvinylpyrrolidone) Nanofibers. *Advances in polymer technology* **2020,** *2020*, 1-9.
22. Popescu, M.-T.; Tasis, D.; Papadimitriou, K. D.; Gkermpoura, S.; Galiotis, C.; Tsitsilianis, C., Colloidal stabilization of graphene sheets by ionizable amphiphilic block copolymers in various media. *RSC Advances* **2015,** *5* (109), 89447-89460.
23. Goenka, S.; Sant, V.; Sant, S., Graphene-based nanomaterials for drug delivery and tissue engineering. *Journal of Controlled Release* **2014,** *173*, 75-88.
24. Liu, M.; Zhang, X.; Wu, W.; Liu, T.; Liu, Y.; Guo, B.; Zhang, R., One-step chemical exfoliation of graphite to ~100% few-layer graphene with high quality and large size at ambient temperature. *Chemical Engineering Journal* **2019,** *355*, 181-185.
25. Kulshrestha, S.; Khan, S.; Meena, R.; Singh, B. R.; Khan, A. U., A graphene/zinc oxide nanocomposite film protects dental implant surfaces against cariogenic Streptococcus mutans. *Biofouling* **2014,** *30* (10), 1281-1294.
26. Zhang, Y.; Nayak, T. R.; Hong, H.; Cai, W., Graphene: a versatile nanoplatform for biomedical applications. *Nanoscale* **2012,** *4* (13), 3833-3842.
27. Nasrollahzadeh, M.; Babaei, F.; Fakhri, P.; Jaleh, B., Synthesis, characterization, structural, optical properties and catalytic activity of reduced graphene oxide/copper nanocomposites. *RSC Advances* **2015,** *5* (14), 10782-10789.
28. Wang, X.; Shi, G., An introduction to the chemistry of graphene. *Physical Chemistry Chemical Physics* **2015,** *17* (43), 28484-28504.
29. Bellunato, A.; Arjmandi Tash, H.; Cesa, Y.; Schneider, G. F., Chemistry at the Edge of Graphene. 2016; Vol. 17, pp 785-801.
30. Xia, W.; Qin, X.; Zhang, Y.; Sinko, R.; Keten, S., Achieving Enhanced Interfacial Adhesion and Dispersion in Cellulose Nanocomposites via Amorphous Interfaces. *Macromolecules* **2018,** *51* (24), 10304-10311.
31. Priyadarsini, S.; Mohanty, S.; Mukherjee, S.; Basu, S.; Mishra, M., Graphene and graphene oxide as nanomaterials for medicine and biology application. *Journal of Nanostructure in Chemistry* **2018,** *8* (2), 123-137.
32. Goodno, B. J.; Gere, J. M., *Mechanics of materials*. Enhanced ninth edition, SI. ed.; Cengage: Boston, MA, 2021.

33. Akpan, E. I.; Shen, X.; Wetzel, B.; Friedrich, K., 2 - Design and Synthesis of Polymer Nanocomposites. In *Polymer Composites with Functionalized Nanoparticles*, Pielichowski, K.; Majka, T. M., Eds. Elsevier: 2019; pp 47-83.
34. Ramakrishna, S.; Huang, Z. M., *9.06 - Biocomposites*. Elsevier Ltd: 2007; Vol. 9, p 215-296.
35. *Nanocomposites with biodegradable polymers : synthesis, properties, and future perspectives*. Oxford University Press: Oxford, 2011.
36. Guangyin, Z.; Youcai, Z., Chapter Five - Harvest of Bioenergy From Sewage Sludge by Anaerobic Digestion. In *Pollution Control and Resource Recovery for Sewage Sludge*, Guangyin, Z.; Youcai, Z., Eds. Butterworth-Heinemann: 2017; pp 181-273.
37. Morel, M. H.; Dehlon, P.; Autran, J. C.; Leygue, J. P.; Bar‐L'Helgouac'h, C., Effects of Temperature, Sonication Time, and Power Settings on Size Distribution and Extractability of Total Wheat Flour Proteins as Determined by Size‐Exclusion High‐Performance Liquid Chromatography. *Cereal chemistry* **2000,** *77* (5), 685-691.
38. Ouyang, Q.; Wang, X.; Xiao, Y.; Luo, F.; Lin, Q.; Ding, Y., Structural changes of A-, B- and C-type starches of corn, potato and pea as influenced by sonication temperature and their relationships with digestibility. *Food chemistry* **2021,** *358*, 129858-129858.
39. Mason, T. J. S. P., Practical Sonochemistry: User's Guide to Applications in Chemistry and Chemical Engineering, Ellis Howood Ldt, New York, 1992. **1998**, 150.
40. William Gilbert, of colchester, physician of London: On the loadstone and magnetic bodies, and on great magnet,the earth. A new physiology demonstrated with many arguments and experiments. A translation by P. Fleury Mottelay. New York: John Wiley & Sons, 53 East Tenth Street. 1893. *Journal of the Franklin Institute* **1893,** *136* (3), 239-239.
41. Tucker, N.; Stanger, J. J.; Staiger, M. P.; Razzaq, H.; Hofman, K., The history of the science and technology of electrospinning from 1600 to 1995. *Journal of engineered fibers and fabrics* **2012,** *7* (3), 63-73.
42. Mouthuy, P. A.; Ye, H., 5.04 - Biomaterials: Electrospinning. In *Comprehensive Biotechnology (Second Edition)*, Moo-Young, M., Ed. Academic Press: Burlington, 2011; pp 23-36.
43. Larrondo, L.; St. John Manley, R., Electrostatic fiber spinning from polymer melts. I. Experimental observations on fiber formation and properties. **1981,** *19* (6), 909-920.
44. Tomer, V.; Teye-Mensah, R.; Tokash, J. C.; Stojilovic, N.; Kataphinan, W.; Evans, E. A.; Chase, G. G.; Ramsier, R. D.; Smith, D. J.; Reneker, D. H., Selective emitters for thermophotovoltaics: erbia-modified electrospun titania nanofibers. *Solar energy materials and solar cells* **2005,** *85* (4), 477-488.
45. Lannutti, J.; Reneker, D.; Ma, T.; Tomasko, D.; Farson, D., Electrospinning for tissue engineering scaffolds. *Materials Science and Engineering: C* **2007,** *27* (3), 504-509.
46. Zhang, C.-L.; Yu, S.-H., Nanoparticles meet electrospinning: recent advances and future prospects. *Chemical Society Reviews* **2014,** *43* (13), 4423-4448.
47. Chronakis, I. S., Novel nanocomposites and nanoceramics based on polymer nanofibers using electrospinning process—A review. *Journal of materials processing technology* **2005,** *167* (2), 283-293.

48. Amith, V.; Sridhar, R.; Angadi, G.; Prajwal, D.; Mamatha, V.; Narasimha Murthy, H. N., Development of Electrospinning System for Synthesis of Polyvinylpyrrolidone Thin Films for Sensor Applications. *Materials Today: Proceedings* **2018,** *5* (10, Part 1), 20920-20926.
49. Jacobs, V.; Anandjiwala, R. D.; Maaza, M., The influence of electrospinning parameters on the structural morphology and diameter of electrospun nanofibers. **2010,** *115* (5), 3130-3136.
50. Tao, J.; Shivkumar, S., Molecular weight dependent structural regimes during the electrospinning of PVA. *Materials Letters* **2007,** *61* (11), 2325-2328.
51. Xue, Q.; Yao, W.; Liu, J.; Tian, Q.; Liu, L.; Li, M.; Lu, Q.; Peng, R.; Wu, W., Facile Synthesis of Silver Nanowires with Different Aspect Ratios and Used as High-Performance Flexible Transparent Electrodes. *Nanoscale research letters* **2017,** *12* (1), 1-12.
52. Hou, J.; Wang, Y.; Xue, H.; Dou, Y., Biomimetic Growth of Hydroxyapatite on Electrospun CA/PVP Core–Shell Nanofiber Membranes. *Polymers* **2018,** *10* (9).
53. Papkov, D.; Zou, Y.; Andalib, M. N.; Goponenko, A.; Cheng, S. Z. D.; Dzenis, Y. A., Simultaneously Strong and Tough Ultrafine Continuous Nanofibers. *ACS nano* **2013,** *7* (4), 3324-3331.
54. Wang, X.; Si, Y.; Wang, X.; Yang, J.; Ding, B.; Chen, L.; Hu, Z.; Yu, J., Tuning hierarchically aligned structures for high-strength PMIA–MWCNT hybrid nanofibers. *Nanoscale* **2013,** *5* (3), 886-889.
55. Zhang, P.; Shao, C.; Li, X.; Zhang, M.; Zhang, X.; Su, C.; Lu, N.; Wang, K.; Liu, Y., An electron-rich free-standing carbon@Au core–shell nanofiber network as a highly active and recyclable catalyst for the reduction of 4-nitrophenol. *Physical Chemistry Chemical Physics* **2013,** *15* (25), 10453-10458.
56. Mack, J. J.; Viculis, L. M.; Ali, A.; Luoh, R.; Yang, G.; Hahn, H. T.; Ko, F. K.; Kaner, R. B., Graphite Nanoplatelet Reinforcement of Electrospun Polyacrylonitrile Nanofibers. **2005,** *17* (1), 77-80.
57. Mayerhöfer, T. G.; Mutschke, H.; Popp, J., Employing Theories Far beyond Their Limits-The Case of the (Boguer-) Beer-Lambert Law. *Chemphyschem* **2016,** *17* (13), 1948-1955.
58. Eaton, P. J.; West, P., *Atomic force microscopy*. Oxford University Press: Oxford ;, 2010.
59. Musielak, M., Red blood cell-deformability measurement: review of techniques. *Clinical hemorheology and microcirculation* **2009,** *42* (1), 47-64.
60. Xu, K.; Sun, W.; Shao, Y.; Wei, F.; Zhang, X.; Wang, W.; Li, P., Recent development of PeakForce Tapping mode atomic force microscopy and its applications on nanoscience. *Nanotechnology Reviews* **2018,** *7* (6), 605-621.
61. Schillers, H.; Medalsy, I.; Hu, S.; Slade, A. L.; Shaw, J. E., PeakForce Tapping resolves individual microvilli on living cells. **2016,** *29* (2), 95-101.
62. You, L., Optimization of the work function measurement by local probe microscopy under vacuum : application to advanced devices. **2012**.
63. Ul-Hamid, A., *A Beginners' Guide to Scanning Electron Microscopy*. 1st ed. 2018. ed.; Springer International Publishing: Cham, 2018.
64. Larkin, P. J., *Infrared and Raman spectroscopy : principles and spectral interpretation*. Second edition. ed.; Elsevier: Amsterdam, Netherlands, 2018.
65. Wu, J.-B.; Lin, M.-L.; Cong, X.; Liu, H.-N.; Tan, P.-H., Raman spectroscopy of graphene-based materials and its applications in related devices. *Chemical Society Reviews* **2018,** *47* (5), 1822-1873.

66. Tabish, T. A.; Pranjol, M. Z. I.; Horsell, D. W.; Rahat, A. A. M.; Whatmore, J. L.; Winyard, P. G.; Zhang, S., Graphene oxide-based targeting of extracellular cathepsin D and Cathepsin L as A Novel anti-metastatic enzyme cancer therapy. *Cancers* **2019,** *11* (3), 319.
67. Pouchert, C. J., *The Aldrich library of FT-IR spectra*. Ed. 2. ed.; Aldrich: Milwaukee, Wis, 1997.
68. Fischer-Cripps, A. C., *Nanoindentation*. 3rd ed. 2011. ed.; Springer New York: New York, NY, 2011.
69. Journal, H. J. C. s., On the Contact of Elastic Solids. *92*, 156-171.
70. Sitharam, T. G.; Govindaraju, L., *Theory of elasticity*. Springer: Singapore, 2021.
71. Fischer-Cripps, A. C., Critical review of analysis and interpretation of nanoindentation test data. *Surface & coatings technology* **2006,** *200* (14-15), 4153-4165.
72. Christöfl, P.; Czibula, C.; Berer, M.; Oreski, G.; Teichert, C.; Pinter, G., Comprehensive investigation of the viscoelastic properties of PMMA by nanoindentation. *Polymer Testing* **2021,** *93*, 106978.
73. Li, X.; Gao, H.; Murphy, C. J.; Caswell, K. K., Nanoindentation of Silver Nanowires. *Nano letters* **2003,** *3* (11), 1495-1498.
74. Zhou, P.; Wu, C.; Li, X., Three-point bending Young's modulus of nanowires. *Measurement Science and Technology* **2008,** *19* (11), 115703.
75. Park, S.; Ruoff, R. S. J. N. N., Chemical methods for the production of graphenes. **2010,** *5*, 309.
76. Kwon, S.; Lee, K. E.; Lee, H.; Koh, S. J.; Ko, J.-H.; Kim, Y.-H.; Kim, S. O.; Park, J. Y., The Effect of Thickness and Chemical Reduction of Graphene Oxide on Nanoscale Friction. *The Journal of Physical Chemistry B* **2018,** *122* (2), 543-547.
77. Borodko, Y.; Habas, S. E.; Koebel, M.; Yang, P.; Frei, H.; Somorjai, G. A., Probing the Interaction of Poly(vinylpyrrolidone) with Platinum Nanocrystals by UV−Raman and FTIR. *The journal of physical chemistry. B* **2006,** *110* (46), 23052-23059.
78. Jaworski, S.; Wierzbicki, M.; Sawosz, E.; Jung, A.; Gielerak, G.; Biernat, J.; Jaremek, H.; Łojkowski, W.; Woźniak, B.; Wojnarowicz, J.; Stobiński, L.; Małolepszy, A.; Mazurkiewicz-Pawlicka, M.; Łojkowski, M.; Kurantowicz, N.; Chwalibog, A., Graphene Oxide-Based Nanocomposites Decorated with Silver Nanoparticles as an Antibacterial Agent. *Nanoscale research letters* **2018,** *13* (1), 116-17.
79. Su, R.; Lin, S. F.; Chen, D. Q.; Chen, G. H., Study on the Absorption Coefficient of Reduced Graphene Oxide Dispersion. *The Journal of Physical Chemistry C* **2014,** *118* (23), 12520-12525.
80. Tais Helena Costa, S.; Christiane Bertachini, L.; Marcos Akira, d. Á., Electrospinning of Gelatin/Poly (Vinyl Pyrrolidone) Blends from Water/Acetic Acid Solutions. *Materials research (São Carlos, São Paulo, Brazil)* **2015,** *18* (3), 509-518.
81. Vollenberg, P. H. T.; Heikens, D., Particle size dependence of the Young's modulus of filled polymers: 1. Preliminary experiments. *Polymer* **1989,** *30* (9), 1656-1662.

Appendices

Appendix A Investigation of Electrospinning Parameters

Table A. 1 Fibre diameter under different electrospinning parameters

Solution Feed Rate (mL/hr)	Applied Voltage (kV)	Collection Distance (cm)	Fibre Diameter (nm)
0.3	8	8	328±82
		9	235±73
		10	204±64
	9	8	315±75
		9	254±65
		10	200±62

Fibres that were electropun at feed rate 0.2 mL/hr and 0.4 mL/hr were present with beads. Also, when applied voltage increased to 10 kV, there were bead formation observed. Therefore, electrospun fibres used these parameters were not included in this Table A.1. The table only includes electrospun fibres at feed rate of 0.3 mL/hr (which allows a stable Taylor cone shape), at applied voltage of 8 kV and 9 kV (which has a minimal bead formation), at different collection distances (8-10 cm).